APOE4 genotype increases neuronal calcium signals and decreases pial arteriole responsivity and vasomotion in visual cortex of awake mice

*Orla Bonnar, Kira Shaw, Dori M. Grijseels, Devin Clarke, Laura Bell, Silvia Anderle, Sarah L. King & Catherine N. Hall**

All affiliations: School of Psychology and Sussex Neuroscience, University of Sussex, Falmer, Brighton, East Sussex, BN1 9RH

*For correspondence please contact Catherine.hall@sussex.ac.uk

ABSTRACT

Vascular dysfunction is an early feature of late onset Alzheimer's disease (AD), preceding classic AD pathology such as beta amyloid accumulation and formation of hyperphosphorylated tau. Such vascular dysfunction may promote classic AD pathology by decreasing blood flow, impairing brain oxygenation and clearance of molecules such as beta amyloid. The main genetic risk factor for AD is the ε4 allele of APOE, which has been found to increase blood brain barrier permeability and decrease vascular density, as well as decrease blood flow and functional hyperaemia in anaesthetised mice undergoing acute surgery. These results suggest that APOE4 may confer AD risk via its effects on the vasculature. However, the responses of neurons and individual vessels have not been studied, so neurovascular relationships are unknown, and no previous studies have looked at awake mice.

We therefore measured neurovascular responses at rest and in response to visual stimulation using 2 photon imaging of awake APOE3 and APOE4 targeted-replacement (APOE TR) mice that expressed the calcium indicator GCaMP6f in excitatory neurons, while labelling the vascular lumen with Texas Red dextran. In parallel, we measured cerebral blood flow, blood oxygenation and cerebral blood volume using combined laser Doppler flowmetry and haemoglobin spectrometry. Measurements were performed in mice aged between 3-4 months to 12-13 months.

We found a milder vascular deficit in awake mice than previous studies that used an acute surgical preparation: capillary responses to visual stimulation were the same in APOE3 and APOE4 TR mice, leading to unimpaired functional hyperaemia. However, neuronal calcium signals during visual stimulation were significantly enhanced in APOE4 mice, while there was a marked decrease in pial arteriole responsiveness and vasomotion. This pattern of results was unaffected by age, suggesting that APOE4 expression creates a stable, but mildly altered neurovascular state that does not itself cause degeneration. However, these changes likely make the system more sensitive to subsequent insults; for example, weaker vasomotion could impair clearance of beta amyloid as it starts to accumulate, and therefore may help explain how APOE4 expression increases risk of developing AD.

Introduction

The brain's dense network of vasculature performs a myriad of roles that are crucial for neuronal health and function, including the fine-tuned delivery of oxygen and glucose via the blood, in response to neuronal activity (neurovascular coupling), and the clearance of waste products from the brain, including CO2 and beta amyloid (Aβ). Both these processes require controlled constriction and dilation of microvascular smooth muscle cells and pericytes. In neurovascular coupling, this likely matches blood flow to energy demand (Iadecola, 2017), while paravascular clearance across the blood brain barrier and along blood vessels is promoted by slow (~0.1Hz) oscillations of arterioles, termed vasomotion (Aldea et al., 2019; Van Veluw et al., 2020). Alterations to these processes are associated with several neurodegenerative diseases, including Alzheimer's disease (AD). In AD, these changes in cerebral blood flow likely establish a vicious cycle that exacerbates AD pathology, whereby decreased blood flow increases Aβ accumulation, by limiting its clearance and promoting its formation in hypoxic conditions. Blood flow is then limited by accumulating Aβ, as blood vessels are constricted by soluble Aβ, lowering flow, and accumulation of Aβ around vessels likely constrains vasomotion (Di Marco et al., 2015; Hamilton et al., 2010; Kisler et al., 2017; Sun et al., 2006; van Veluw et al., 2020). In fact, vascular dysregulation has been shown to be among the earliest pathologies found in AD (Iturria-Medina et al., 2016), so these changes may critically shape the emergence of AD pathology.

Whilst the majority of AD cases are sporadic, the risk of going on to develop the disease is increased 9-15 fold by the possession of an ε4 allele of the apolipoprotein E (APOE) gene (Corder et al., 1993; Yamazaki et al., 2019). ApoE is a protein involved in the transport of lipids and is produced primarily by astrocytes in the CNS, but also by neurons under stress conditions, vascular mural cells and microglia (Kanekiyo et al., 2014). APOE4 expression results in numerous deleterious effects in AD, including increased Aβ accumulation, enhanced tau phosphorylation and synaptic alterations (Najm et al., 2019). Among these effects are vascular changes that result in loss of BBB integrity, pericyte and endothelial cell damage and reduced cerebral blood flow (CBF) responses to sensory stimulation (Bell et al., 2012; Montagne et al., 2020; Rieker et al., 2019; Koizumi et al., 2018). We were interested in whether these vascular pathologies may start to explain how possession of the APOE4 allele increases risk of developing AD, so sought to determine how effective vasoconstriction and dilation of pericytes and smooth muscle cells was in mice expressing human APOE4 compared to APOE3 at baseline and in response to neuronal activity. We also wanted to better understand whether altered vascular responses reflected different underlying neuronal activity, and whether any changes were exacerbated with age, paralleling the increasing risk with age for humans developing AD.

This study is, to our knowledge, the first to examine the effect of ApoE4 on the vasculature in vivo, without the confounding effects of anaesthesia, as well as to study neuronal activity and vascular function in the same animals. Unlike studies using anaesthetised mice, we found many vascular parameters to be preserved in APOE4 mice (e.g. the magnitude of vascular responses to sensory stimulation, net haemodynamic responses to stimulation and baseline blood oxygenation). However, there was a consistent decrease in the reliability of vasodilation in response to neuronal activity, a reduction in the slow oscillations that are known to be

important drivers of paravascular clearance, and a marked increase in the size of excitatory calcium signals during visual stimulation in APOE4 compared to APOE3 animals. These effects were not modulated by age. Therefore, our results suggest that APOE4 expression produces several subtle alterations to the neurovascular function that are not in themselves sufficient to cause degeneration, but render them susceptible to further vascular pathology, particularly at the intersection with other factors such as increased inflammation, hypertension or the presence of Aβ or hyperphosphorylated tau.

Results

Reduced vascular density in young APOE4 TR mice is not reflected in baseline flow and blood oxygenation.

Studies using anaesthetised preparations have previously shown decreased vascular density and cerebral blood flow in APOE4 compared to APOE3 TR mice (Bell et al., 2012; Koizumi et al., 2018). We confirmed the reduction in vascular density in the visual cortex of 3-4 month APOE4 TR mice using fixed brain tissue with the vasculature filled with a fluorescent gelatin (Fig. 1A, B). We then tested the impact of this reduction in vascular density on various aspects of haemodynamic function in awake mice with a cranial window implanted over the visual cortex, at rest and in the absence of visual stimulation (hereafter referred to as 'baseline' conditions; Fig. 1C). In vivo measures of red blood cell velocity (RBCV; Fig. 1D, E) and haematocrit (Fig. 1D, G) did not differ between genotypes, nor did the diameters of individual capillaries (Fig. 1H) or of pial vessels feeding the microvasculature (Fig. 1I). The coefficient of variation, reflecting temporal fluctuations in RBCV, trended towards being significant (Fig. 1G). An increase in temporal variation suggests heterogeneity in capillary flow which may indicate less efficient oxygen extraction (Angleys et al., 2015). However, neither RBC flux or sO_2 (measured using laser Doppler flowmetry (LDF) and haemoglobin spectroscopy respectively) were different between genotypes in this baseline condition (Fig. 1J, K). Therefore, the decrease in vascular density is not sufficient, in these mice, to drive net alterations in regional CBF or blood oxygenation, despite the absence of compensatory alterations in the diameter, RBC content or flow in individual vessels.

Neuronal activity is unchanged at baseline, but APOE4 TR animals display a hyperactive phenotype in response to visual stimulation.

To allow visualisation of neuronal activity during in vivo 2 photon imaging, we bred APOE-TR mice with Thy1-GCaMP6f, to generate mice which expressed GCaMP6f in excitatory neurons (Dana et al., 2014) and were homozygous for APOE3 or APOE4 in place of murine APOE. We imaged visual cortical calcium signals (Fig. 2A) during baseline and during presentation of a drifting grating (Fig. 1C) and detected calcium events as peaks in the fluorescence signal in each region of interest (ROI) normalised to baseline (Fig. 2B), as well as measuring the overall calcium response across all ROIs during visual stimulation. There were no differences between genotypes in the number of calcium peaks per minute (Fig. 2C) and the size of these peaks

during baseline conditions (Fig. 2D). In contrast, the change in fluorescence in response to a visual stimulation was enhanced in APOE4 TR mice (Fig. 2E, F), though the number of cells that significantly increased their calcium during visual stimulation was unchanged (Fig. 2G). Therefore, calcium signals increase more in cells responsive to a visual stimulus in APOE4 compared to APOE3 TR mice. This effect could be due to increased depolarisation or spiking of these cells during visual stimulation, or increased calcium entry to the same level of electrical excitation. Both options are plausible: calcium handling has been shown to be impaired in astrocytes of male APOE4 TR mice (Larramona-Arcas et al., 2020), while neurons of old APOE4 TR mice have been shown to be hyperactive due to decreased inhibitory GABAergic tone (Nuriel et al., 2017).

Vascular responses to visual stimulation are unimpaired in the capillary bed, but pial arterioles are less responsive in APOE4 TR mice.

We were interested whether the alterations in pericyte function previously reported to increase BBB permeability (Bell et al., 2012) would also affect the ability of vessels to respond to increased neuronal activity during visual stimulation. We therefore measured vascular diameter changes in response to stimulation in pial arterioles and downstream capillaries, as well as stimulus-evoked changes in RBCV in capillaries. In a healthy system, visual stimulation evokes neuronal activity in the visual cortex and blood flow to the area increases accordingly, seen as increased dilations in capillaries and upstream pial vessels, and an increase in RBCV in individual vessels (Fig. 3E, A, I). The frequency and size of dilations in response to visual stimulation was the same in the capillary bed of APOE3 and APOE4 TR mice (Fig. 3F, G, H). However, the frequency of upstream pial dilations was decreased in APOE4 TR mice, as was the percentage of vessels with RBCV responses (Fig. 3D, L). Furthermore, the size of these responses, when they did occur, was no different between genotypes (Fig. 3B, C, J, K), suggesting the potential for dilation remained the same in both genotypes. This was also the case when the size of the response was normalised to the larger neuronal responses in APOE4 vs APOE3 TR mice (Supplementary Figure S1). Because vasodilation propagates upstream from the capillary bed (Chen et al., 2014; Iadecola et al., 1997), this decreased reliability of APOE4 TR mice pial vessels in the absence of changes in capillary responsiveness may suggest an impairment in the propagation of dilation from the capillaries, rather than in the capacity of pericytes and smooth muscle cells to dilate.

To test whether these alterations in vascular responsivity affected macroscopic haemodynamic response, we also compared the CBF, sO_2 and blood volume (total haemoglobin: HbT) responses to visual stimulation, but these were no different between genotypes (Supplementary Figure S2). The neurovascular changes observable at the single vessel level are therefore not, in these conditions, sufficient to affect these macroscopic measurements of neurovascular coupling. The lack of a genotype effect on overall CBF is consistent with the unimpaired capillary responses, as the capillary bed represents the majority of the resistance in the vascular bed, so is expected to mediate most of the increase in CBF during functional hyperaemia (Blinder et al., 2013; Hall et al., 2014).

APOE4 TR mice have impaired vasomotion

Arteries and arterioles oscillate at low frequencies (~0.1Hz) — a phenomenon termed vasomotion (Mayhew et al., 1996). In addition to being indicative generally of vascular function and health, vasomotion has also been shown to be one of the drivers of clearance from the brain (van Veluw et al., 2020) and is altered in mouse models of Alzheimer's disease (Di Marco et al., 2015). As AD, and indeed APOE4, is associated with a reduction in clearance of Aβ, we tested whether vasomotion in pial arterioles was affected by APOE genotype. Fourier transforms of our diameter traces (Fig. 4A) decompose the time course of diameter changes into a spectrum of the power of fluctuations at different frequencies, revealing peaks of increased power at vasomotion frequencies at 0.1Hz – 0.3Hz (Fig. 4B). However, the power at these frequencies was strikingly lower in APOE4 mice (Fig. 4C), quantified by measuring the power at 0.1Hz (Fig. 4D). This was not because of differences in locomotion during recording (Fig. 4E). We explored these differences in more detail using a recently published method (Fitting oscillations and one over f: FOOOF; Donoghue et al., 2020) to parameterise the power spectra into aperiodic and periodic components (Fig. 4F). There was a lower aperiodic component of the power spectra in APOE4 TR animals (Fig. 4G) and the magnitude (but not the frequency) of the largest low frequency peaks (those larger than 3.5 x standard deviations of all peaks (Fig. 4H), see methods) was also lower in these mice (Fig. 4 I, J).

It has been demonstrated by others that vasomotion, although an intrinsic vascular property, can be entrained by neuronal activity (Mateo et al., 2017), in particular the gamma band envelope. We carried out Fourier analyses on GCaMP data, which although acquired at too low a frequency to measure gamma band activity, can reveal neuronal oscillatory activity that correlates with vasomotion (He et al., 2018). Not only was there no peak in the neuronal power spectrum in the vasomotion range (Fig. 4K), but the power did not differ between genotypes (Fig. 4L), and there was no alteration to the aperiodic component (Fig. 4M). There was a very large variability in the APOE4 TR calcium power spectra, but this was clearly not reduced at low frequencies relative to the APOE3 TR signals, suggesting that the observed reduction in oscillatory activity in APOE4 mice is likely vascular rather than neuronal in origin, at least as far as can be reflected in excitatory neuronal calcium signals. There were no genotype differences in the power spectra for any net measures of haemodynamic activity or for RBCV (Supplementary Figure S3).

Age does not modulate neurovascular alterations in APOE4 animals.

Vascular and neuronal reactivity to visual stimulation was then measured at older time points, to determine if age affected neurovascular function. Due to availability of appropriate transgenic mice, neuronal activity was only additionally measured in mice aged 6-7 months, while vascular features were measured in mice aged 6-7 months and 12-13 months. No age-related decreases in function were recorded in any of the parameters measured (Fig. 5A-F). In addition, taken across the whole age range, the frequency of increases in RBCV to visual stimulation was no longer significantly lower in APOE4 compared to APOE3 TR mice (Fig. 5I) and as in young animals, the response frequency of capillary diameters did not differ by genotype (Fig. 5H). The decrease in response frequency of pial arterioles remained significantly lower in

APOE4 mice (Fig. 5G), however, as did the impaired vasomotion of these vessels (Fig. 6A-C), as reflected in the lower power at 0.1Hz (Fig. 6D). A parameterised fit of these power spectra revealed a consistently lower aperiodic component in APOE4 mice across the ages studied (Fig. 6E), while the peak fitted in this way showed an interaction between genotype and age, being larger in APOE4 mice at older ages (Fig. 6F), with no alterations to peak frequency across ages or genotypes (Fig. 6G). However, because the power is clearly much lower overall in the APOE4 mice (Fig. 6A-C), and the FOOOF method fits noise as well as clear peaks at low frequencies (Supplementary Figure S4), we are not confident this accurately reflects the periodic component of these traces. Thus, there is a large decrease in low-frequency vasomotion of pial arteriole diameters across the lifespan in APOE4 TR mice, with irregular, aperiodic fluctuations being clearly lower in APOE4 TR mice. The properties of oscillatory, periodic fluctuations need further investigation.

We confirmed that genotype differences were not because of differences in locomotion activity during recordings or differences in model fits (Supplementary Figures S4-6). Neuronal calcium remained enhanced in APOE4 TR mice during visual stimulation at the older age studied (Fig. 5J, K), without any alterations to the response frequency of neurons (Fig. 5K, L). These data suggest that neurovascular function in APOE3 and APOE4 TR mice is rather stable, showing specific and persistent differences in pial arteriole responsivity, irregular vasomotion and neuronal function across the lifespan into early old age.

Discussion

This was the first study to elucidate the effect of APOE genotype on neurovascular function at single neuron and vessel resolution, and in awake mice. Generally, we found milder effects of APOE4 genotype than has been previously suggested. While vascular density was reduced in APOE4 mice, this did not affect baseline CBF, blood sO_2, or RBCV in single capillaries. Regional increases in blood flow, sO_2 or blood volume, or the size of single vessel dilations in response to visual stimulation were also not affected (unlike previously found, Koizumi et al., 2018). Pial arterioles were, however, less likely to dilate to visual stimulation, and showed decreased vasomotion in APOE4 compared to APOE3 TR mice. Furthermore, unlike previously reported overall reductions in neuronal activity (Bell et al., 2012), we found an increase in neuronal calcium signals during visual stimulation. These genotype differences were broadly unaffected by age, suggesting they represent a stable state that does not, itself, cause progressive dysfunction. These effects may, instead, interact with other factors to place the system more at risk of dysfunction when external events do occur (e.g., age, infection).

Differences with previous studies

Koizumi et al found a large decrease in the CBF response to whisker stimulation in APOE4 TR mice (Koizumi et al., 2018), while Bell et al found a decrease in neuronal activity in response to hind limb stimulation, measured with voltage dyes (Bell et al., 2012). Although a regional difference between somatosensory and visual cortex cannot be ruled out, a more likely mechanism is the difference in experimental preparation. In our experiments, animals are

imaged while awake and alert, having been allowed to recover from surgery for at least two weeks. The other studies utilised an acute preparation in which the mouse underwent cranial window surgery and was still anaesthetised when neuronal or haemodynamic recordings were undertaken. As mouse models of disease can be more susceptible to cortical spreading depression after invasive surgery (Shabir et al., 2020), and APOE4 is associated with an enhanced inflammatory phenotype (Kloske and Wilcock, 2020), the increased pathology observed in acute preparations may be due to this increased sensitivity to surgery and/or anaesthesia. Our findings, that there is an enhancement of neuronal activity and a slight disruption of vascular function, are a much closer approximation to the mild changes seen in young to middle-aged human APOE4 carriers (Henson et al., 2020; O'Donoghue et al., 2018).

Physiological impact of APOE4 changes in neurovascular function

We initially hypothesised that the mild changes we observed in young animals might progress into worse pathology with age. We wondered if the increased neuronal activity, suggesting an increased energy demand, might be insufficiently provided for by the less responsive vasculature leading to an energy imbalance that could eventually drive neuronal and vascular damage. Our data suggest that this is not the case, however. The alterations in neuronal and vascular function remained largely stable from 4 to 12-13 months of age. Instead, therefore, our data suggest that APOE4 TR mice are different from APOE3 TR mice in specific, subtle but consistent ways. This parallels findings in humans of the existence of subtle differences between healthy APOE3 and 4 carriers (higher default mode network functional connectivity in APOE4s), but the lack of age-dependent changes in any measures studied, from cognition to brain structure (Henson et al., 2020) . The genotype differences do not, therefore, cause significant or progressive pathology in healthy, active individuals (our mice are housed in an enriched environment with access to an exercise wheel), but may cause APOE4 carriers (mice or humans) to be more sensitive to triggers that can then cause progression into a pathophysiological state. Such a trigger could be acute surgeries under anaesthetic, as discussed above, experimental interventions such as decreased cerebral perfusion (Koizumi et al., 2018), environmental changes such as exposure to infection, extreme age or, as in the two-hit hypothesis of AD , factors that initiate the accumulation of Aβ (Zlokovic, 2011).

A key issue for future research is then to untangle how existing differences between APOE3 and 4 carriers interact with additional triggers to cause a change from a stable state to progressive pathology and neurodegeneration. Because cardiovascular risk factors potentiate the risk of someone carrying an APOE4 allele developing AD (Juul Rasmussen et al., 2020), vascular factors are likely involved in this switch, while neuronal changes that could potentiate production of Aβ are also relevant. Some such differences are already known, including increased BBB permeability and pericyte inflammation (Bell et al., 2012; Montagne et al., 2020). Our results add three further features for consideration: increased neuronal calcium signals, decreased pial vessel responsivity, and decreased pial vasomotion.

Neuronal calcium: Before our study, increased neuronal calcium levels have been previously reported in cultured neurons exposed to ApoE4 both at rest and in response to stimulation

(NMDA application, Qiu et al., 2003; or mechanical injury, Jiang et al., 2015; though in the latter, ApoE4 had no effect on resting calcium). Whether or not these observations and the increased signals we measure in vivo are due to increased neuronal depolarisation or altered calcium handling (as has been found in APOE4-positive astrocytes from male mice; Larramona-Arcas et al., 2020), the ubiquity of the involvement of calcium in cellular processes means that these alterations are likely to be physiologically relevant. The increase in calcium, and its ability to modulate synaptic strengths could therefore potentially underlie the increased connectivity and gamma band oscillations observed in human APOE4 carriers (Henson et al., 2020). It will be of interest to observe how such circuit changes develop in mice, to determine whether this contributes to the decrease in GABAergic inhibitory tone and electrophysiological hyperactivity that develops in old age APOE4 mice (Nuriel et al., 2017). Of particular interest is how these alterations affect how neurons respond to Aβ. Neuronal hyperactivity increases in response to Aβ, but predominantly in cells that are already active (Zott et al., 2019). Therefore, increased neuronal activity caused by ApoE4 may magnify the hyperactivity caused when Aβ is produced, exacerbating its pathophysiological effects.

Pial arteriole responsiveness: In our experiments, pial arterioles in APOE4 TR mice dilated less frequently to visual stimulation. These alterations in pial responsiveness were not sufficient to reduce the overall regional increase in CBF, HbT or oxygen delivery but do indicate something is different in the pial vasculature of these APOE4 TR mice. Because the capillary bed responses were unchanged, and the pial dilations when they did occur were also of the same size in APOE3 and APOE4 TR mice, we suppose that the capacity of the smooth muscle cells and pericytes of APOE4 TR mice to dilate was not impaired, but possibly instead the ability of dilations to spread upstream from the capillary bed to trigger upstream pial dilations. A future research question would be whether endothelial calcium signals are altered as well as those in neurons, as these signals are involved in propagation of vasodilation via activation of transient receptor potential ankyrin 1 (TRPA1; Thakore et al., 2021) as well as activating nitric oxide production, which itself can modulate propagation of vasodilation (Kovacs-Oller et al., 2020) .

Pial arteriole vasomotion: Possibly the most striking difference between APOE3 and APOE4 TR mice was the decrease in low frequency fluctuations of pial arteriole diameter in APOE4 mice - a phenomenon known as vasomotion. Vasomotion can be oscillatory or irregular (Wagner and Persson, 1998). Parameterising the aperiodic and periodic components of the power spectra revealed a consistent reduction in the aperiodic component, alongside a less consistent alteration in the periodic component. The inconsistent effects on the periodic component may be because at the low frequencies studied here (< 1Hz), the peaks in the power spectrum were hard to distinguish from noise that was also fitted by the FOOOF algorithm (see Supplementary Figure S4). Nevertheless, the clear finding is that low frequency fluctuations, including aperiodic (non-oscillatory) vasomotion, are impaired in APOE4 compared to APOE3 TR mice.

The mechanism underlying this reduced vasomotion is unclear, especially as we show that smooth muscle cells can dilate to neuronal activity, with similar size responses to stimulation in APOE4 mice. Though vasomotion has been found to entrain to neuronal activity (Mateo et al., 2017), we find no evidence of a reduced neuronal drive on vasomotion, though this should be

confirmed with electrophysiological measurements of local field potentials, to directly examine the gamma band envelope thought to entrain vasomotion. The relevance of the difference in the aperiodic component of vasomotion is also unclear. In the periphery, aperiodic vasomotion has been shown not to require the endothelium (Griffith and Edwards, 1994), and may be due to the interaction of two oscillating pathways that regulate intracellular calcium levels in smooth muscle cells (influx through voltage-gated channels and efflux via the sodium-calcium exchanger and ryanodine receptor-mediated release from intracellular stores; Wagner and Persson, 1998). APOE4-mediated variations in calcium handling could alter these interactions to reduce vasomotion, but this requires experimental investigation. Other contributions to aperiodic vasomotion have also been proposed from neuronal modulation, blood pressure and autoregulation (Wagner and Persson, 1998; Cavalcanti and Ursino, 1996).

Whatever the underlying mechanism, our results may help us understand how, in APOE4 carriers, a system with reduced vasomotion could be stable, but at risk of decline if Aβ production increases. This is because vasomotion is thought to be important for paravascular clearance of waste molecules, including Aβ, from the brain (Weller et al., 2008; Van Veluw et al., 2020). APOE4 carriers have already been shown to have an increased Aβ burden both in AD and in cerebral amyloid angiopathy (CAA), probably as a result of reduced clearance (Greenberg et al., 2020). Whilst there are several mechanisms that have been shown to contribute to this, including reduced clearance across the BBB (Deane et al., 2008) and reduced degradation (Jiang et al., 2008; Miners et al., 2006), our data and others (Hawkes et al., 2012) point towards reduced paravascular clearance, due to a decreased driving force from vasomotion, as an additional mechanism. Thus, reduced vasomotion may not matter for the normal physiological functioning of the brain until Aβ production increases and clearance fails, allowing Aβ to accumulate further and exacerbate vascular dysfunction.

Conclusion

Together our data point towards a subtle yet robust effect of APOE4 on the neurovascular system across the lifetime. They indicate APOE4 TR mice have increased neuronal calcium signals in response to sensory stimulation that may contribute to the altered network activity observed in humans and older mice. Our data also reveal specific deficits in pial arteriole responsiveness and vasomotion that are not on their own sufficient to alter oxygen delivery or cerebral blood flow in healthy mice. However, the nature of these changes suggests that they may be important features that contribute to the decline of the previously stable system when an additional challenge is encountered, be that further vascular damage, infection or initiation of Aβ accumulation. These genotype effects on neuronal and vascular function may therefore partially explain how the APOE4 genotype confers risk of developing AD.

Materials and Methods

Animals

All experimental procedures were approved by the UK Home Office, in accordance with the 1986 Animal (Scientific Procedures) Act, under a project licence held by C.H.. All experiments were carried out on homozygous APOE3-TR or APOE4-TR mice (Sullivan et al., 1997), crossed with animals expressing DsRed under the control of the NG2 promoter (Zhu et al., 2008) or with animals expressing GCaMP6f under the control of the Thy1 promoter. All animals were on a C57BL/6 background. Both male and female mice were used in this study. Mice were between 3-4 months old unless otherwise specified. In ageing experiments, 6-7 month mice were the same as those imaged earlier at 3-4 months, while 12-13 month mice were a separate cohort. Animals were housed in a temperature-controlled room with a 12-hour light/dark cycle and had free access to food and water.

Surgical Preparation

Animals were surgically implanted with a cranial window over the primary visual cortex as previously described (Shaw et al., 2019). Briefly, animals were anaesthetised with isoflurane (~4% at induction, ~1.5 – 2% maintenance) and body temperature was maintained at 37°C using a homeothermic monitoring system (PhysioSuite, Kent Scientific Corporation). A 3 mm hole was created over the visual cortex, the dura removed, and a glass window used to seal the exposed area. Custom made titanium head bars were fixed to the exposed skull to later facilitate head fixation. Animals were administered subcutaneous injections of saline 0.9% (400µL), buprenorphine (1.2µg, Vetergesic, Ceva), meloxicam (6.2 µg, Metacam, Boehringer Ingelheim) and dexamethasone (120 µg, Dexadreson, MSD Animal Health) at induction, and continued to receive meloxicam (100 µg) in food for three days post-surgery.

In vivo experiments

For all in vivo experiments, animals were head-fixed atop a cylindrical treadmill and locomotion was recorded using a rotary encoder (Kuebler). Recordings were made during both 'baseline' conditions (~4 minutes per recording), defined as the absence of visual stimulation with the animal free to engage in locomotion, and during visual stimulation (~ 8 minutes per recording). A drifting grating (315°, 2Hz full screen stimulus, with alternating spatial frequency trials of either 0.04 or 0.2 cycles per degree) was presented for 5 seconds on screens (Asus, ~17cm from mouse), with an interstimulus interval of 20 seconds, slowing for stimulus triggered responses to be measured.

2 photon microscopy

Animals were imaged using a two-photon microscope (Scientifica) and a mode-locked Ti-sapphire laser (Coherent). Images were acquired using a 20x (XLUMPlanFL N, Olympus) or 16x (LWD, Nikon) water immersion objective from tissue excited at with a laser wavelength of 940nm or 970 nm. The objective was shielded with light occluding tape to minimise light artefacts from visual stimulation. Images were collected using SciScan (Scientifica) software, at an acquisition rate of 3.8-7.6 frames per second for x-y recordings, and at an average acquisition rate of 1221 lines per second, for high-speed line scan recordings.

Prior to imaging, animals were injected with a fluorescent dextran. Those with green fluorescence (i.e., GCaMP6f) were injected with 2.5% Texas red (Sigma-Aldrich) either subcutaneously (3 kDa) or intravenously via the tail vein (70 kDa), and those with red fluorescence (i.e., DsRed in vascular mural cells) were injected intravenously with 2.5% fluorescein isothiocyanate-dextran (70 kDa FITC-dextran; Sigma-Aldrich)), allowing for visualisation of the vasculature. Pial arterioles were identified by the presence of smooth muscle cells (in NG2-DSred animals), or by their morphology and orientation relative to the large pial veins, as well as their response to visual stimulation. Pial arterioles were then followed with recordings made (average pixel size: 0.42 µm) after bifurcations, until the vessels penetrated the parenchyma and therefore would no longer be classed as pial. Penetrating arterioles were followed and branching capillaries were imaged using high speed line scans, to record both diameter and RBCV (average pixel size: 0.20 µm). In animals positive for GCaMP6f, x-y recordings (256x256 pixels; average pixel size: 1.28µm) were taken from the area proximate to vessel recordings at a depth that allowed for clear visualisation of neuronal cell bodies (layer 2/3 (~z = -150µm)).

Oxy-CBF probe

Net haemodynamic measurements were recorded using a combined laser Doppler flowmetry/ haemoglobin spectroscopy probe (Oxy-CBF probe; Moor Instruments; Royl et al., 2008) at an acquisition rate of 40 Hz. Net measures of total haemoglobin (Hbt), blood flow (flux) and oxygen saturation (sO_2) were obtained both at baseline and during visual stimulation.

In vivo data analysis

Vascular diameter and RBCV measurements

Prior to analysis, several preprocessing steps were carried out in ImageJ (FIJI) to improve the quality of images as required. Such adjustments included registration, despeckling and/or median 3D filtering. In addition, all images had the 'stack contrast adjustment' plug-in applied to minimise any light artifacts arising from the visual stimulation. A custom MATLAB script was written to analyse vessel diameter using the full width at half maximum (Shaw, 2021). Briefly, a skeleton was generated along the centre of each vessel and an intensity profile was generated along a line perpendicular to the vessel. Values were obtained across a window of five pixels

and averaged to obtain a mean value per window. This was repeated at every second skeleton point, allowing for diameter measurements to be made along the full vascular arbour. These measurements were then averaged along the vessel, resulting in an average diameter per frame.

Similar methods were used to measure the diameter of capillaries imaged using high speed line scans, but rather than measuring across 5-pixel windows, measurements were obtained across windows of 40ms. Red blood cell velocity measurements were calculated with a radon transform using freely available code (Drew et al., 2010) . In brief, the angle of shadows cast by the RBCs (that do not uptake fluorescent dextran) were measured and used to calculate the velocity across 40ms time windows that overlapped by 10 ms. Angles that were extremely large or small (because of motion artefacts) were removed. To further account for noise in the data obtained from line scans, traces went through either one (diameter) or two (RBCV) iteration(s) of outlier removal. In addition, for stimulation experiments, trials missing greater than 10% of data were excluded and those that remained were subsequently smoothed using a loess smoothing method (range: 1-5% span of the total number of data points, depending on which best represented the shape of the data). To determine AUC measurements, data was interpolated to fill in missing values, using a moving mean average.

A coefficient of variation was calculated for RBCV for each individual vessel, to measure temporal variation, by dividing the standard deviation over time by the mean value. Images acquired of shadows cast by RBCs were binarised and the percentage area taken up by RBCs was calculated (black pixels vs. white pixels) to give a value for haematocrit.

Neuronal fluorescence measurements

Regions of interest (ROIs) over neurons were identified in GCaMP6f recordings, using the freely available software Suite2p (Pachitariu et al., 2016). A fluorescence signal was extracted from each ROI, along with a background measure (F_{neu}). To reduce out-of-focus neuropil contamination of the signal, 0.7 x F_{neu} was subtracted from each ROI (Chen et al., 2013).

Baseline analysis (no visual stimulation)

Baseline measures of neuronal activity were computed in rest epochs of at least 10 seconds by counting peaks per minute and the size of these peaks. To find peaks in the calcium signal, traces were first scaled so that all values fell between zero and one (equation a). Peaks were then identified as being at least twice the standard deviation of the whole trace, and 0.25 seconds apart from the next peak. Each original trace was then normalised as is standard, (equation b) and the size of each peak was determined. This process was carried out per ROI, which were subsequently averaged per animal.

(a) $\Delta F/F = (F-F_{min})/(F_{max} - F_{min})$

(b) $\Delta K/K = (K-K_0)/abs(K_0)$

F represents the fluorescence trace. K represents the data trace (fluorescence or diameter), and K_0 represents the baseline period to which the rest of the data is normalised.

For haemodynamic measures at baseline that were recorded in the absence of a visual stimulation, rest periods were found as above for neuronal activity and an average value per vessel or animal (as specified in individual figure legends) was calculated for each measured parameter.

Visual stimulation data analysis

Neuronal and vessel diameter data acquired from visual stimulation experiments were cut into trials around the stimulus presentations and averaged to yield a mean response per vessel or animal, as specified in figure legends. Only trials where there was no significant locomotion during the period two seconds prior to stimulation onset or during the stimulation period were used. Significant locomotion was defined as an event that was more than one third of a second in length and/or less than one second apart from adjacent locomotion epochs.

Data were normalised to the 5 s baseline preceding the onset of visual stimulation using equation (a). To determine if there was a response to stimulation, a threshold was set as twice the standard deviation of this 5 s baseline period (Supplementary Figure S7). Any response larger than this threshold was deemed 'responsive'. For neuronal data all trials were averaged per ROI and if the mean response was larger than the threshold, it was deemed a responsive ROI and subsequently averaged to provide a mean per animal. A percentage response rate was thus obtained per vessel or animal. For vascular data, these trials were averaged per vessel to provide a 'responsive only' trace. Each vessel had a different number of contributing trials (because mice ran different amounts for each recording) and those with a low number of trials were likely to provide more extreme response frequency values (e.g., 0% or 100%). Therefore, the number of contributing trials per vessel was used to weight data when calculating response frequency. Area under the curve (AUC) measurements were taken during the stimulation period using the inbuilt MATLAB function "trapz" which utilizes trapezoidal numerical integration. Neurovascular coupling indices (NVCi) were calculated by dividing each vascular AUC by the average neuronal AUC for each genotype (as some mice expressed DsRed in pericytes and did not express GCaMP6f in neurons, so calcium data was not available for each mouse).

Power spectrum analysis

Welch's power spectral density estimates were computed across all traces (including locomotion epochs) for arteriole diameters, calcium fluorescence traces, RBCV measurements and net sO_2 and CBF measurements. All data was detrended by subtracting the baseline (the 8th percentile calculated over 15 second time windows (Supplementary Figure S8; Dombeck et al, 2010). Discrete Fourier transforms were then carried out across 60 second time windows using the inbuilt MATLAB function "pwelch". Resulting power spectra were corrected for 1/f noise. Data below 1 Hz was selected and interpolated to the same length using linear

interpolation (Supplementary Figure S8). All data underwent outlier removal based on the value at 0.1Hz (all values greater than 3 standard deviations above the mean were removed). This resulted in the removal of a total of three pial arteriole traces, no calcium traces, two RBCV traces and one trace for both sO_2 and HbT. The power spectra were subsequently parameterised into aperiodic and periodic components using a recently published algorithm (Donoghue et al., 2020). The algorithm was set using the following parameters: peak width limits: *0.03-0.2 Hz*; max number of peaks: default (infinite), minimum peak height: default (0), peak threshold: 1; and aperiodic mode: 'knee', across the frequency range 0.06 to 0.95 Hz. The model fits for all data, as well as the aperiodic offsets are shown in Supplementary Figures S4, S6 and S9. A threshold for peak height (a periodic output) was set to detect only the largest peaks. Different thresholds were explored in Supplementary Figure S4 with a threshold of 3.5 times the standard deviation selected. Aperiodic curves were plotted using equation (c):

(c) $\log(\text{Power}) = Re(\text{offset} - \log(\text{knee} + \text{frequency}^{\text{exponent}}))$

Fixed tissue

APOE TR mice with DsRed expression driven by the NG2 promoter, underwent transcardial perfusion under terminal anaesthesia. Animals were first perfused with 0.1 M phosphate buffered saline (PBS) then 4% paraformaldehyde (PFA) in PBS, and were then perfused with 5% gelatin containing 0.2% FITC-conjugated albumin (at 37 °C). Following at least 30 minutes on ice, brain tissue was then extracted and stored in 4% PFA at 4˚C for 24 hours before being transferred to 30% sucrose in PBS for at least 3 days. Tissue was then sliced at 200µm on a vibratome, and slices were imaged using confocal microscopy (Leica SP8). Vascular density was calculated from the length of vascular skeleton per unit volume, using the "Analyse Skeleton" plugin in FIJI/ImageJ (Arganda-Carreras et al., 2010) .

Statistics

Statistical analyses were conducted in GraphPad Prism 8, SPSS, RStudio and MATLAB. Data are presented as mean +/- SEM. Individual data points represent individual blood vessels, brain slices or animals as specified in figure legends. Data whose residuals were normally distributed, as determined by a D'Agostino-Pearson and Shapiro-Wilk test, were compared using an unpaired t test, with a Welch's correction applied if variances were unequal as determined by an F test. Data that were not normally distributed were compared using a non-parametric Mann-Whitney U test. Linear mixed models (LMM) were carried out using 'lmer' in RStudio, with random effects specified in figure legends. For correlation analyses, normally distributed data were analysed using Pearson's correlation, and non-normal data were analysed using Spearman's rank correlation. To weight response frequency data, so that vessels with a larger number of contributing trials contributed more to the mean, a weighted least squares linear regression was used and the mean was weighted by the number of contributing trials. Finally, where multiple comparisons were made, p-values were adjusted using Tukey's correction or a

Bonferroni-Dunn correction, as specified in the figure legends. P values below 0.05 were considered significant and those below 0.1 as trending towards significance.

Funding: This work was funded by an Alzheimer's Society DTC PhD studentship to O.B., Sussex Neuroscience PhD studentships for D.G. and D.C., the MRC (MR/S026495/1; MC_PC_15071) and an Academy of Medical Sciences/Wellcome Trust Springboard award to C.N.H..

Bibliography

Aldea R, Weller RO, Wilcock DM, Carare RO, Richardson G. 2019. Cerebrovascular smooth muscle cells as the drivers of intramural periarterial drainage of the brain. *Front Aging Neurosci* **11**:1. doi:10.3389/fnagi.2019.00001

Angleys H, Østergaard L, Jespersen SN. 2015. The effects of capillary transit time heterogeneity (CTH) on brain oxygenation. *J Cereb Blood Flow Metab* **35**:806–817. doi:10.1038/jcbfm.2014.254

Arganda-Carreras I, Fernández-González R, Muñoz-Barrutia A, Ortiz-De-Solorzano C. 2010. 3D reconstruction of histological sections: Application to mammary gland tissue. *Microsc Res Tech* **73**:1019–1029. doi:10.1002/jemt.20829

Bell RD, Winkler EA, Singh I, Sagare AP, Deane R, Wu Z, Holtzman DM, Betsholtz C, Armulik A, Sallstrom J, Berk BC, Zlokovic BV. 2012. Apolipoprotein E controls cerebrovascular integrity via cyclophilin A. *Nature* **485**:512–516. doi:10.1038/nature11087

Blinder P, Tsai PS, Kaufhold JP, Knutsen PM, Suhl H, Kleinfeld D. 2013. The cortical angiome: an interconnected vascular network with noncolumnar patterns of blood flow. *Nat Neurosci* **16**:889–897. doi:10.1038/nn.3426

Cavalcanti S, Ursino M. 1996. Chaotic oscillations in microvessel arterial networks. *Ann Biomed Eng* **24**:37–47. doi:10.1007/BF02770993

Chen BR, Kozberg MG, Bouchard MB, Shaik MA, Hillman EMC. 2014. A critical role for the vascular endothelium in functional neurovascular coupling in the brain. *J Am Heart Assoc* **3**:e000787. doi:10.1161/JAHA.114.000787

Chen T-W, Wardill TJ, Sun Y, Pulver SR, Renninger SL, Baohan A, Schreiter ER, Kerr RA, Orger MB, Jayaraman V, Looger LL, Svoboda K, Kim DS. 2013. Ultrasensitive fluorescent proteins for imaging neuronal activity. *Nature* **499**:295–300. doi:10.1038/nature12354

Corder EH, Saunders AM, Strittmatter WJ, Schmechel DE, Gaskell PC, Small GW, Roses AD, Haines JL, Pericak-Vance MA. 1993. Gene dose of apolipoprotein E type 4 allele and the risk of Alzheimer's disease in late onset families. *Science* **261**:921–923. doi:10.1126/science.8346443

Dana H, Chen T-W, Hu A, Shields BC, Guo C, Looger LL, Kim DS, Svoboda K. 2014. Thy1-GCaMP6 transgenic mice for neuronal population imaging in vivo. *PLoS ONE* **9**:e108697. doi:10.1371/journal.pone.0108697

Deane R, Sagare A, Hamm K, Parisi M, Lane S, Finn MB, Holtzman DM, Zlokovic BV. 2008. apoE isoform – specific disruption of amyloid β peptide clearance from mouse brain. *The Journal of Clinical Investigation* **118**:4002–4013.

Di Marco LY, Farkas E, Martin C, Venneri A, Frangi AF. 2015. Is vasomotion in cerebral arteries impaired in alzheimer's disease? *J Alzheimers Dis* **46**:35–53. doi:10.3233/JAD-142976

Dombeck DA, Harvey CD, Tian L, Looger LL, Tank DW. 2010. Functional imaging of hippocampal place cells at cellular resolution during virtual navigation. *Nat Neurosci* **13**:1433–1440. doi:10.1038/nn.2648

Donoghue T, Haller M, Peterson EJ, Varma P, Sebastian P, Gao R, Noto T, Lara AH, Wallis JD, Knight RT, Shestyuk A, Voytek B. 2020. Parameterizing neural power spectra into periodic and aperiodic components. Nat Neurosci 23:1655–1665. doi:10.1038/s41593-020-00744-x

Drew PJ, Blinder P, Cauwenberghs G, Shih AY, Kleinfeld D. 2010. Rapid determination of particle velocity from space-time images using the Radon transform. *J Comput Neurosci* **29**:5–11. doi:10.1007/s10827-009-0159-1

Greenberg SM, Bacskai BJ, Hernandez-Guillamon M, Pruzin J, Sperling R, van Veluw SJ. 2020. Cerebral amyloid angiopathy and Alzheimer disease - one peptide, two pathways. *Nat Rev Neurol* **16**:30–42. doi:10.1038/s41582-019-0281-2

Griffith TM, Edwards DH. 1994. EDRF suppresses chaotic pressure oscillations in isolated resistance artery without influencing intrinsic complexity. *Am J Physiol* **266**:H1786-800. doi:10.1152/ajpheart.1994.266.5.H1786

Grijseels DM, Shaw K, Barry C, Hall CN. 2021. Choice of method of place cell classification determines the population of cells identified. *BioRxiv*. doi:10.1101/2021.02.26.433025

Hall CN, Reynell C, Gesslein B, Hamilton NB, Mishra A, Sutherland BA, O'Farrell FM, Buchan AM, Lauritzen M, Attwell D. 2014. Capillary pericytes regulate cerebral blood flow in health and disease. *Nature* **508**:55–60. doi:10.1038/nature13165

Hamilton NB, Attwell D, Hall CN. 2010. Pericyte-mediated regulation of capillary diameter: a component of neurovascular coupling in health and disease. *Front Neuroenergetics* **2**. doi:10.3389/fnene.2010.00005

Hawkes CA, Sullivan PM, Hands S, Weller RO, Nicoll JAR, Carare RO. 2012. Disruption of arterial perivascular drainage of amyloid-β from the brains of mice expressing the human APOE ε4 allele. *PLoS ONE* **7**:e41636. doi:10.1371/journal.pone.0041636

Henson RN, Suri S, Knights E, Rowe JB, Kievit RA, Lyall DM, Chan D, Eising E, Fisher SE. 2020. Effect of apolipoprotein E polymorphism on cognition and brain in the Cambridge Centre for Ageing and Neuroscience cohort. *Brain Neurosci Adv* **4**:2398212820961704. doi:10.1177/2398212820961704

He Y, Wang M, Chen X, Pohmann R, Polimeni JR, Scheffler K, Rosen BR, Kleinfeld D, Yu X. 2018. Ultra-Slow Single-Vessel BOLD and CBV-Based fMRI Spatiotemporal Dynamics and Their Correlation with Neuronal Intracellular Calcium Signals. *Neuron* **97**:925-939.e5. doi:10.1016/j.neuron.2018.01.025

Iadecola C, Yang G, Ebner TJ, Chen G. 1997. Local and propagated vascular responses evoked by focal synaptic activity in cerebellar cortex. *J Neurophysiol* **78**:651–659. doi:10.1152/jn.1997.78.2.651

Iadecola C. 2017. The Neurovascular Unit Coming of Age: A Journey through Neurovascular Coupling in Health and Disease. *Neuron* **96**:17–42. doi:10.1016/j.neuron.2017.07.030

Iturria-Medina Y, Sotero RC, Toussaint PJ, Mateos-Pérez JM, Evans AC, Alzheimer's Disease Neuroimaging Initiative. 2016. Early role of vascular dysregulation on late-onset Alzheimer's disease based on multifactorial data-driven analysis. *Nat Commun* **7**:11934. doi:10.1038/ncomms11934

Jiang L, Zhong J, Dou X, Cheng C, Huang Z, Sun X. 2015. Effects of ApoE on intracellular calcium levels and apoptosis of neurons after mechanical injury. *Neuroscience* **301**:375–383. doi:10.1016/j.neuroscience.2015.06.005

Jiang Q, Lee CYD, Mandrekar S, Wilkinson B, Cramer P, Zelcer N, Mann K, Lamb B, Willson TM, Collins JL, Richardson JC, Smith JD, Comery TA, Riddell D, Holtzman DM, Tontonoz P, Landreth GE. 2008. ApoE promotes the proteolytic degradation of Abeta. *Neuron* **58**:681–693. doi:10.1016/j.neuron.2008.04.010

Juul Rasmussen I, Rasmussen KL, Nordestgaard BG, Tybjærg-Hansen A, Frikke-Schmidt R. 2020. Impact of cardiovascular risk factors and genetics on 10-year absolute risk of dementia: risk charts for targeted prevention. *Eur Heart J* **41**:4024–4033. doi:10.1093/eurheartj/ehaa695

Kanekiyo T, Xu H, Bu G. 2014. ApoE and Aβ in Alzheimer's disease: accidental encounters or partners? *Neuron* **81**:740–754. doi:10.1016/j.neuron.2014.01.045

Kisler K, Nelson AR, Montagne A, Zlokovic BV. 2017. Cerebral blood flow regulation and neurovascular dysfunction in Alzheimer disease. *Nat Rev Neurosci* **18**:419–434. doi:10.1038/nrn.2017.48

Kloske CM, Wilcock DM. 2020. The important interface between apolipoprotein E and neuroinflammation in alzheimer's disease. *Front Immunol* **11**:754. doi:10.3389/fimmu.2020.00754

Koizumi K, Hattori Y, Ahn SJ, Buendia I, Ciacciarelli A, Uekawa K, Wang G, Hiller A, Zhao L, Voss HU, Paul SM, Schaffer C, Park L, Iadecola C. 2018. Apoε4 disrupts neurovascular regulation and undermines white matter integrity and cognitive function. *Nat Commun* **9**:3816. doi:10.1038/s41467-018-06301-2

Kovacs-Oller T, Ivanova E, Bianchimano P, Sagdullaev BT. 2020. The pericyte connectome: spatial precision of neurovascular coupling is driven by selective connectivity maps of pericytes and endothelial cells and is disrupted in diabetes. *Cell Discov* **6**:39. doi:10.1038/s41421-020-0180-0

Shaw, K. Brain Energy Lab. 2021. BrainEnergyLab/HCvsV1_NVC_Manuscript: NVCinHCmanuscript_March2021_release1. *Zenodo*. doi:10.5281/zenodo.4593010

Larramona-Arcas R, González-Arias C, Perea G, Gutiérrez A, Vitorica J, García-Barrera T, Gómez-Ariza JL, Pascua-Maestro R, Ganfornina MD, Kara E, Hudry E, Martinez-Vicente M, Vila M, Galea E, Masgrau R. 2020. Sex-dependent calcium hyperactivity due to lysosomal-related dysfunction in astrocytes from APOE4 versus APOE3 gene targeted replacement mice. *Mol Neurodegener* **15**:35. doi:10.1186/s13024-020-00382-8

Mateo C, Knutsen PM, Tsai PS, Shih AY, Kleinfeld D. 2017. Entrainment of Arteriole Vasomotor Fluctuations by Neural Activity Is a Basis of Blood-Oxygenation-Level-Dependent "Resting-State" Connectivity. *Neuron* **96**:936-948.e3. doi:10.1016/j.neuron.2017.10.012

Mayhew JE, Askew S, Zheng Y, Porrill J, Westby GW, Redgrave P, Rector DM, Harper RM. 1996. Cerebral vasomotion: a 0.1-Hz oscillation in reflected light imaging of neural activity. *Neuroimage* **4**:183–193. doi:10.1006/nimg.1996.0069

Miners JS, Van Helmond Z, Chalmers K, Wilcock G, Love S, Kehoe PG. 2006. Decreased expression and activity of neprilysin in Alzheimer disease are associated with cerebral amyloid angiopathy. *J Neuropathol Exp Neurol* **65**:1012–1021. doi:10.1097/01.jnen.0000240463.87886.9a

Montagne A, Nation DA, Sagare AP, Barisano G, Sweeney MD, Chakhoyan A, Pachicano M, Joe E, Nelson AR, D'Orazio LM, Buennagel DP, Harrington MG, Benzinger TLS, Fagan AM, Ringman JM, Schneider LS, Morris JC, Reiman EM, Caselli RJ, Chui HC, Zlokovic BV. 2020. APOE4 leads to blood-brain barrier dysfunction predicting cognitive decline. *Nature* **581**:71–76. doi:10.1038/s41586-020-2247-3

Najm R, Jones EA, Huang Y. 2019. Apolipoprotein E4, inhibitory network dysfunction, and Alzheimer's disease. *Mol Neurodegener* **14**:24. doi:10.1186/s13024-019-0324-6

Nuriel T, Angulo SL, Khan U, Ashok A, Chen Q, Figueroa HY, Emrani S, Liu L, Herman M, Barrett G, Savage V, Buitrago L, Cepeda-Prado E, Fung C, Goldberg E, Gross SS, Hussaini SA, Moreno H, Small SA, Duff KE. 2017. Neuronal hyperactivity due to loss of inhibitory tone in APOE4 mice lacking Alzheimer's disease-like pathology. *Nat Commun* **8**:1464. doi:10.1038/s41467-017-01444-0

O'Donoghue MC, Murphy SE, Zamboni G, Nobre AC, Mackay CE. 2018. APOE genotype and cognition in healthy individuals at risk of Alzheimer's disease: A review. *Cortex* **104**:103–123. doi:10.1016/j.cortex.2018.03.025

Pachitariu M, Stringer C, Schröder S, Dipoppa M, Rossi LF, Carandini M, Harris KD. 2016. Suite2p: beyond 10,000 neurons with standard two-photon microscopy. *BioRxiv*. doi:10.1101/061507

Qiu Z, Crutcher KA, Hyman BT, Rebeck GW. 2003. ApoE isoforms affect neuronal N-methyl-D-aspartate calcium responses and toxicity via receptor-mediated processes. *Neuroscience* **122**:291–303. doi:10.1016/j.neuroscience.2003.08.017

Rieker C, Migliavacca E, Vaucher A, Baud G, Marquis J, Charpagne A, Hegde N, Guignard L, McLachlan M, Pooler AM. 2019. Apolipoprotein E4 Expression Causes Gain of Toxic Function in Isogenic Human Induced Pluripotent Stem Cell-Derived Endothelial Cells. *Arterioscler Thromb Vasc Biol* **39**:e195–e207. doi:10.1161/ATVBAHA.118.312261

Royl G, Füchtemeier M, Leithner C, Megow D, Offenhauser N, Steinbrink J, Kohl-Bareis M, Dirnagl U, Lindauer U. 2008. Hypothermia effects on neurovascular coupling and cerebral metabolic rate of oxygen. *Neuroimage* **40**:1523–1532. doi:10.1016/j.neuroimage.2008.01.041

Shabir O, Pendry B, Lee L, Eyre B, Sharp P, Rebollar MA, Howarth C, Heath PR, Wharton SB, Francis SE, Berwick J. 2020. Assessment of neurovascular coupling & cortical spreading depression in mixed models of atherosclerosis & alzheimer's disease. *BioRxiv*. doi:10.1101/2020.08.13.249987

Shaw K, Bell L, Boyd K, Grijseels DM, Clarke D, Bonnar O, Crombag HS, Hall CN. 2019. Hippocampus has lower oxygenation and weaker control of brain blood flow than cortex, due to microvascular differences. *BioRxiv*. doi:10.1101/835728

Sullivan PM, Mezdour H, Aratani Y, Knouff C, Najib J, Reddick RL, Quarfordt SH, Maeda N. 1997. Targeted replacement of the mouse apolipoprotein E gene with the common human APOE3 allele enhances diet-induced hypercholesterolemia and atherosclerosis. *J Biol Chem* **272**:17972–17980. doi:10.1074/jbc.272.29.17972

Sun X, He G, Qing H, Zhou W, Dobie F, Cai F, Staufenbiel M, Huang LE, Song W. 2006. Hypoxia facilitates Alzheimer's disease pathogenesis by up-regulating BACE1 gene expression. *Proc Natl Acad Sci USA* **103**:18727–18732. doi:10.1073/pnas.0606298103

Thakore P, Alvarado MG, Ali S, Mughal A, Pires PW, Yamasaki E, Pritchard HA, Isakson BE, Tran CHT, Earley S. 2021. Brain endothelial cell TRPA1 channels initiate neurovascular coupling. *elife* **10**. doi:10.7554/eLife.63040

van Veluw SJ, Hou SS, Calvo-Rodriguez M, Arbel-Ornath M, Snyder AC, Frosch MP, Greenberg SM, Bacskai BJ. 2020. Vasomotion as a driving force for paravascular clearance in the awake mouse brain. *Neuron* **105**:549-561.e5. doi:10.1016/j.neuron.2019.10.033

Wagner CD, Persson PB. 1998. Chaos in the cardiovascular system: an update. *Cardiovasc Res* **40**:257–264. doi:10.1016/s0008-6363(98)00251-x

Weller RO, Subash M, Preston SD, Mazanti I, Carare RO. 2008. Perivascular drainage of amyloid-beta peptides from the brain and its failure in cerebral amyloid angiopathy and Alzheimer's disease. *Brain Pathol* **18**:253–266. doi:10.1111/j.1750-3639.2008.00133.x

Yamazaki Y, Zhao N, Caulfield TR, Liu C-C, Bu G. 2019. Apolipoprotein E and Alzheimer disease: pathobiology and targeting strategies. *Nat Rev Neurol* **15**:501–518. doi:10.1038/s41582-019-0228-7

Zhu X, Bergles DE, Nishiyama A. 2008. NG2 cells generate both oligodendrocytes and gray matter astrocytes. *Development* **135**:145–157. doi:10.1242/dev.004895

Zlokovic BV. 2011. Neurovascular pathways to neurodegeneration in Alzheimer's disease and other disorders. *Nat Rev Neurosci* **12**:723–738. doi:10.1038/nrn3114

Zott B, Simon MM, Hong W, Unger F, Chen-Engerer H-J, Frosch MP, Sakmann B, Walsh DM, Konnerth A. 2019. A vicious cycle of β amyloid-dependent neuronal hyperactivation. *Science* **365**:559–565. doi:10.1126/science.aay0198

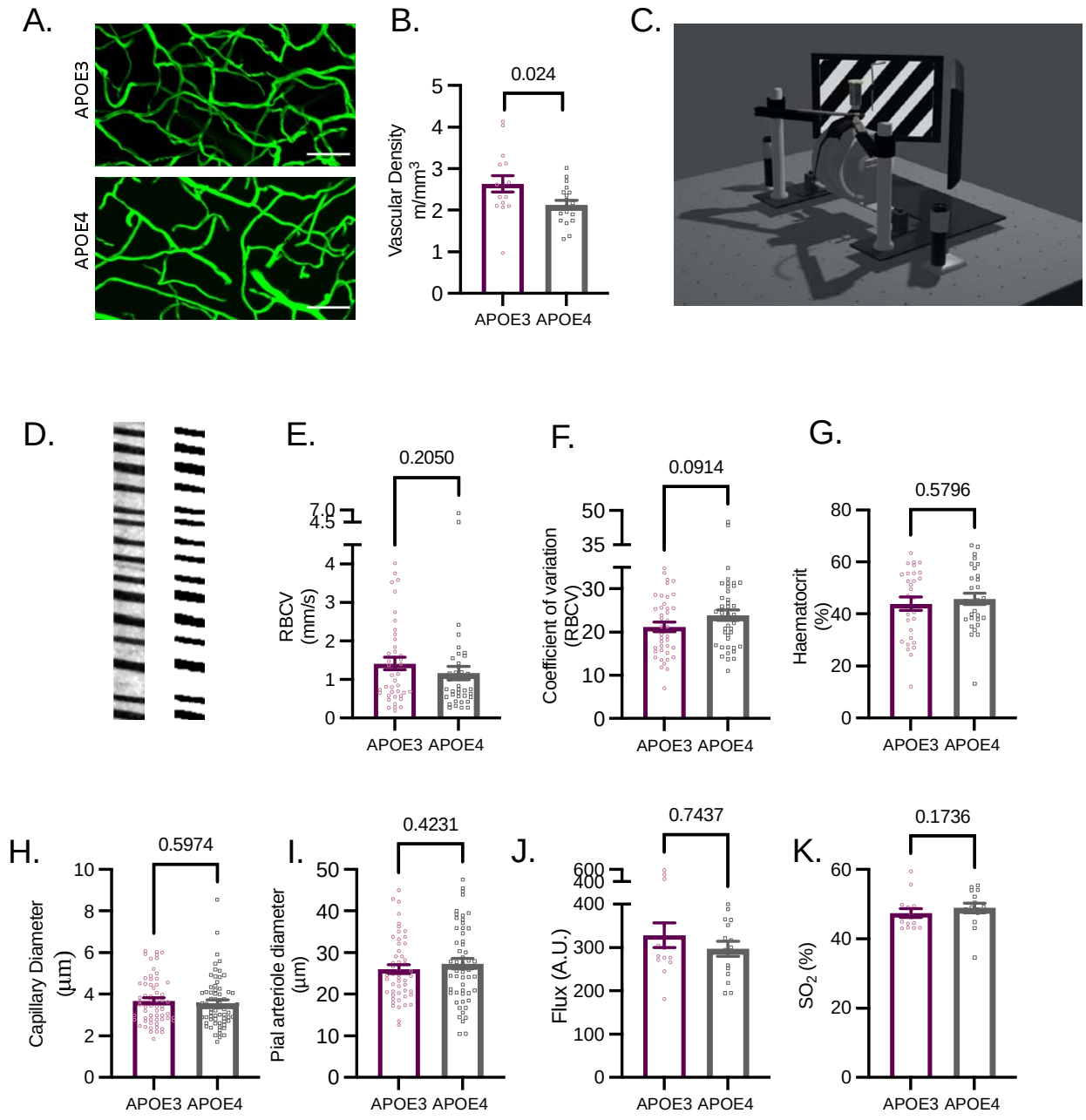

Figure 1. Under baseline conditions functional measurements are largely preserved in APOE4 mice, but vascular density is reduced. **A)** Example z-projected images of FITC-gelatin perfused vessels (green) from the visual cortex. Scale bars: 50 µm. Z depth: 45.6 µm. **B)** Vascular density

(of vessels <10 µm in diameter) was reduced in APOE4 animals. **C)** Schematic of in vivo imaging set up. Screens delivered visual stimulation (drifting grating). Net haemodynamic measurements were recorded using the Oxy-CBF probe and individual vessels and neurons were imaged using 2 photon microscopy. Figure adapted from Grijseels et al (2021); (D) Example output from a capillary line scan after preprocessing (left) and the same image binarised (right) for haematocrit measurements. No genotype differences were found in RBCV **(E)** or in haematocrit **(G)** measures but a trend towards increased RBCV coefficient of variation (CV) was observed in APOE4 animals **(F)**. No genotype differences were observed in capillary or pial arteriole diameters **(H, I)** net measurements of flux **(J)** or SO_2 **(K).** Data are shown as mean ± SEM. P values were obtained from t-tests (F, G, I) or Mann Whitney U tests (E, H, J, K) or from LMM with animal included as a random factor (B). Sample sizes were as follows (APOE3/APOE4): **(B)** n = 16/19 slices, 3/3 animals. **(C)** n = 52/55 vessels, 15/15 animals. (**E, F)** n = 42/41 vessels, 12/12 animals. **(G)** n = 29/30 vessels, 11/11 animals. **(H, I)** n = 15/15 animals.

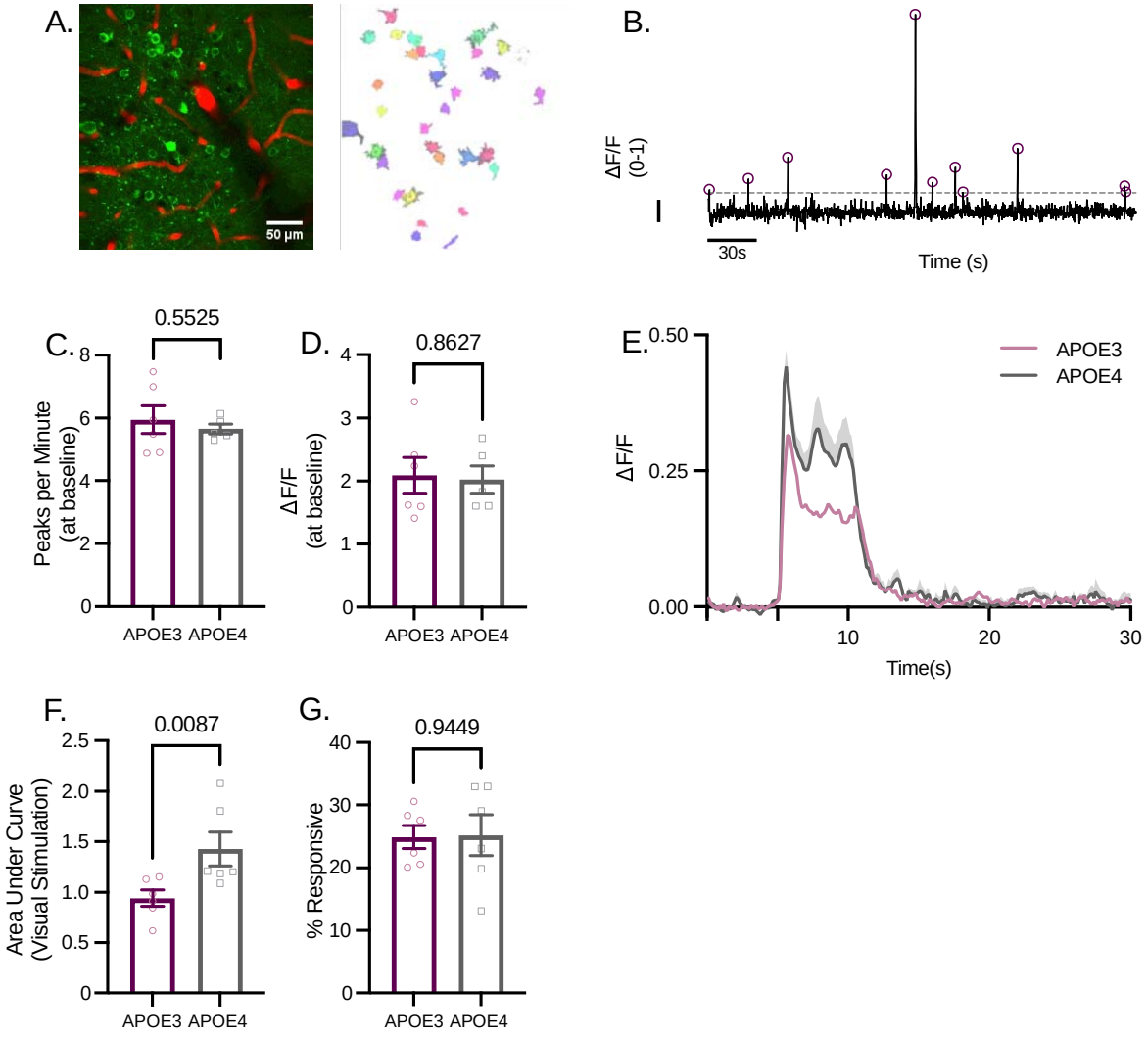

Figure 2. Under baseline conditions, genotypes display the same neuronal characteristics, but during visual stimulation APOE4 animals have larger neuronal responses. **A)** Left: Thy1-GCaMP expressing neurons (green) and Texas Red filled vasculature (red) from visual cortex. Right: ROIs detected using Suite2P (Pachitariu et al; 2016). **B)** Example ΔF/F trace from one ROI, normalised between 0-1. Dashed line depicts threshold for peak selection, circles represent detected peaks and scale bar represents ΔF/F of 0.1 on the y axis and 30 s on the x axis. At baseline, the number of detected peaks **(C)** and the size of those peaks **(D)** did not differ between genotypes. The size of the neuronal response to visual stimulation (blue shaded region) was larger in APOE4 animals **(E, F)** but the percentage of neurons that responded to visual stimulation did not differ between genotypes **(G)**. Data are shown as mean ± SEM. P values were obtained from t-tests (with Welch's correction where variances were unequal) (C, D, G) or Mann Whitney U tests (F). APOE3/APOE4: (C, D) n = 1770/1677 cells, 6/5 animals. (F) n = 503/593 cells, 6/6 animals. (G) n = 1943/2140 cells, 6/6 animals.

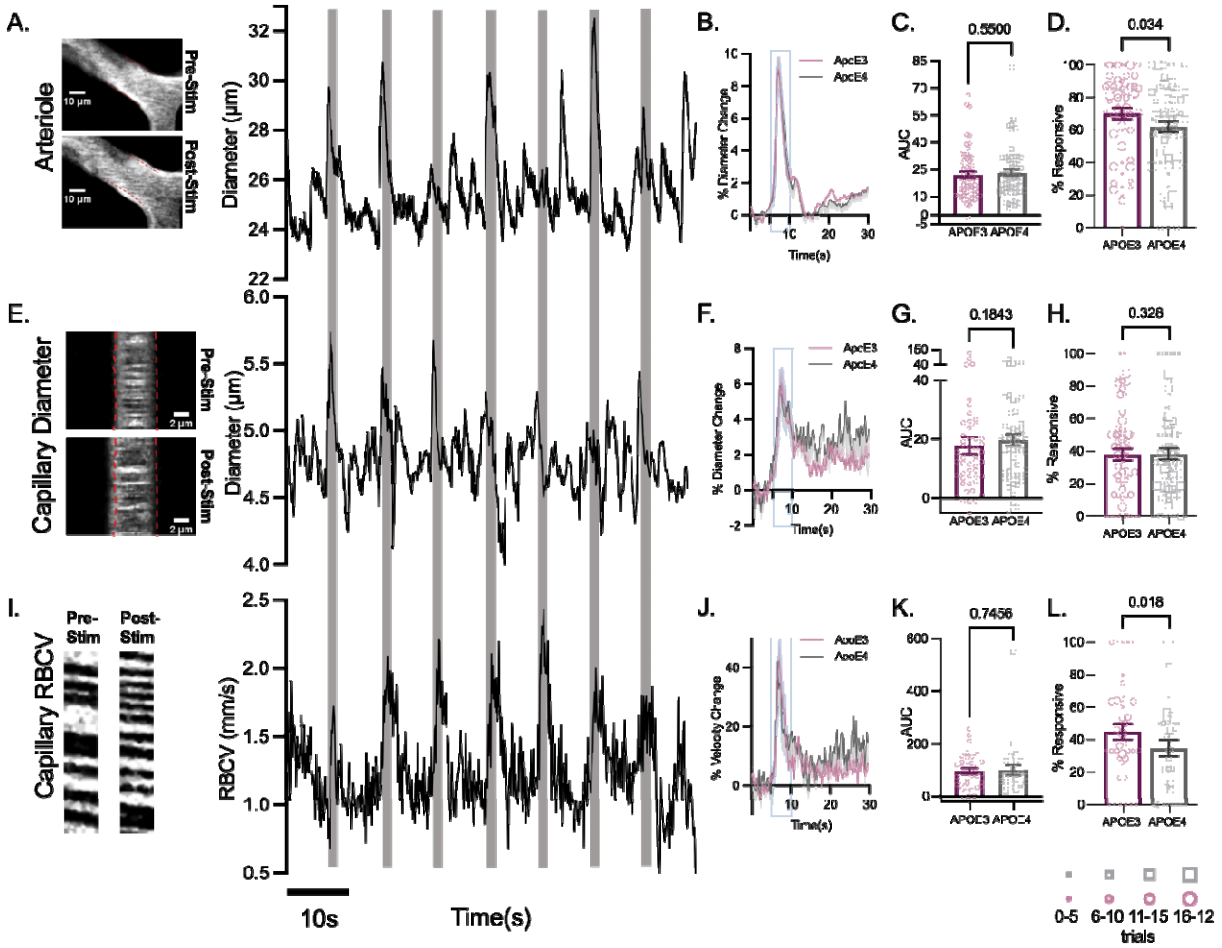

Figure 3. Vascular responses to visual stimulation are less reliable in APOE4 mice, but response sizes do not differ between genotypes. Example images and time series traces of pial arteriole diameter **(A)**, capillary diameter **(E)** and capillary RBCV **(I)** responses to visual stimulation. The response magnitude did not differ between genotypes in either the arteriole diameter **(B, C)**, capillary diameter **(F, G)** or capillary RBCV **(J, K)**. In APOE4 mice, the pial arteriole **(D)** and RBCV **(L)** response frequency was reduced, however there was no difference in the frequency of response to visual stimulation in capillary diameters **(H)**. Response frequency was weighted according to the number of contributing trials per vessel. The size of the individual data points reflects the number of trials, as per legend. Data are shown as mean ± SEM. P values were obtained from Mann Whitney U tests (C, G, K) or WLS linear regression (weighted by number of contributing trials) (D, H, L). APOE3/APOE4: (C, D) n = 59/61 vessels, 15/15 animals. (G, H) n = 51/62 vessels, 12/13 animals. (K, L) n = 39/37, 12/11 animals.

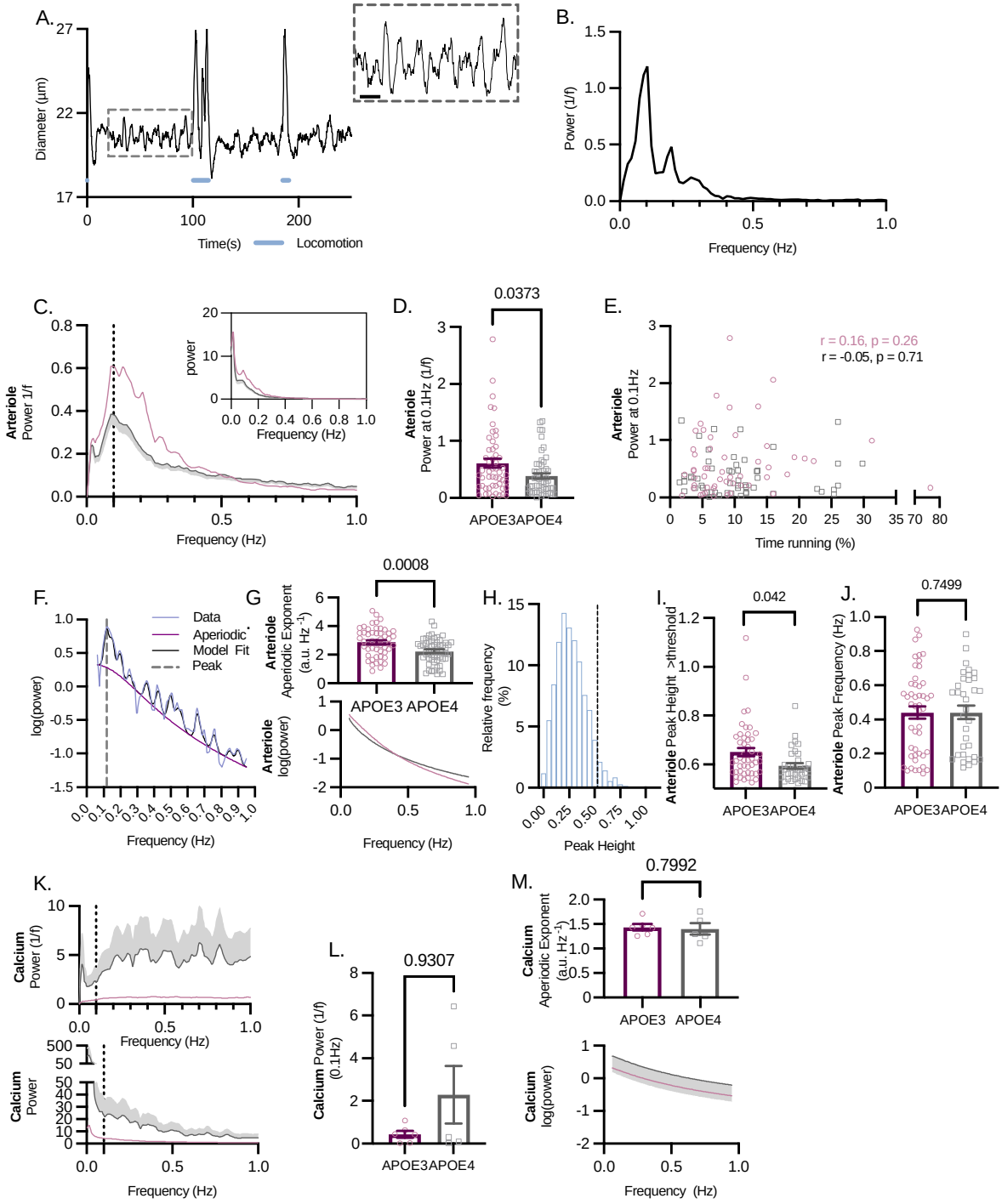

Figure 4. Vasomotion is reduced in APOE4 mice. **A).** Example arteriole diameter trace showing spontaneous fluctuations in diameter (see insert) in the absence of locomotion or sensory stimulation. **B)** Power spectrum of diameter trace shown in A. Peak frequency can be observed

at ~0.1Hz. **C)** Average power spectra of diameter traces from APOE3 and APOE4 mice. Main figure shows power spectra normalised for 1/f noise, insert shows unnormalised traces. Dashed line at 0.1Hz. **D)** APOE4 mice have lower power at 0.1Hz. **E)** The power at 0.1Hz was not affected by the amount of time spent running for either genotype. **F)** Example output from FOOOF (Donoghue et al, 2020**)**. **(G)** APOE4 power spectra had a smaller aperiodic component as shown by the value of the aperiodic exponent (top panel) as well as the average aperiodic curves (bottom panel). **H)** A histogram of all peaks detected by FOOOF, across both genotypes. Dashed line shows threshold (3.5 x standard deviation of all peaks), above which peaks were analysed. Peak height was reduced in APOE4 mice **(I)**, however the frequency spread of the peaks **(J)** did not differ. **K)** Average power spectra for thy1-GCaMP6f fluorescence in APOE3 and APOE4 animals. Top panel shows spectra normalised for 1/f noise, bottom shows unnormalised traces. There was no difference in the power at 0.1Hz **(L)**, or in the aperiodic component of the spectra **(M)** as measured by FOOOF. Data are shown as mean ± SEM. p values were obtained from Mann Whitney U tests (D, J), t-tests (with Welch's correction where variances were unequal) (G, L, M), Spearman's rank correlation (E) and LMM with vessel ID as a random factor. APOE3/APOE4: (D, E, G) n = 52/53 vessels, 15/15 animals. (I, J) n = 47/34 detected peaks, 12/14 animals. (L, M) n = 1770/1677 cells, 6/5 animals.

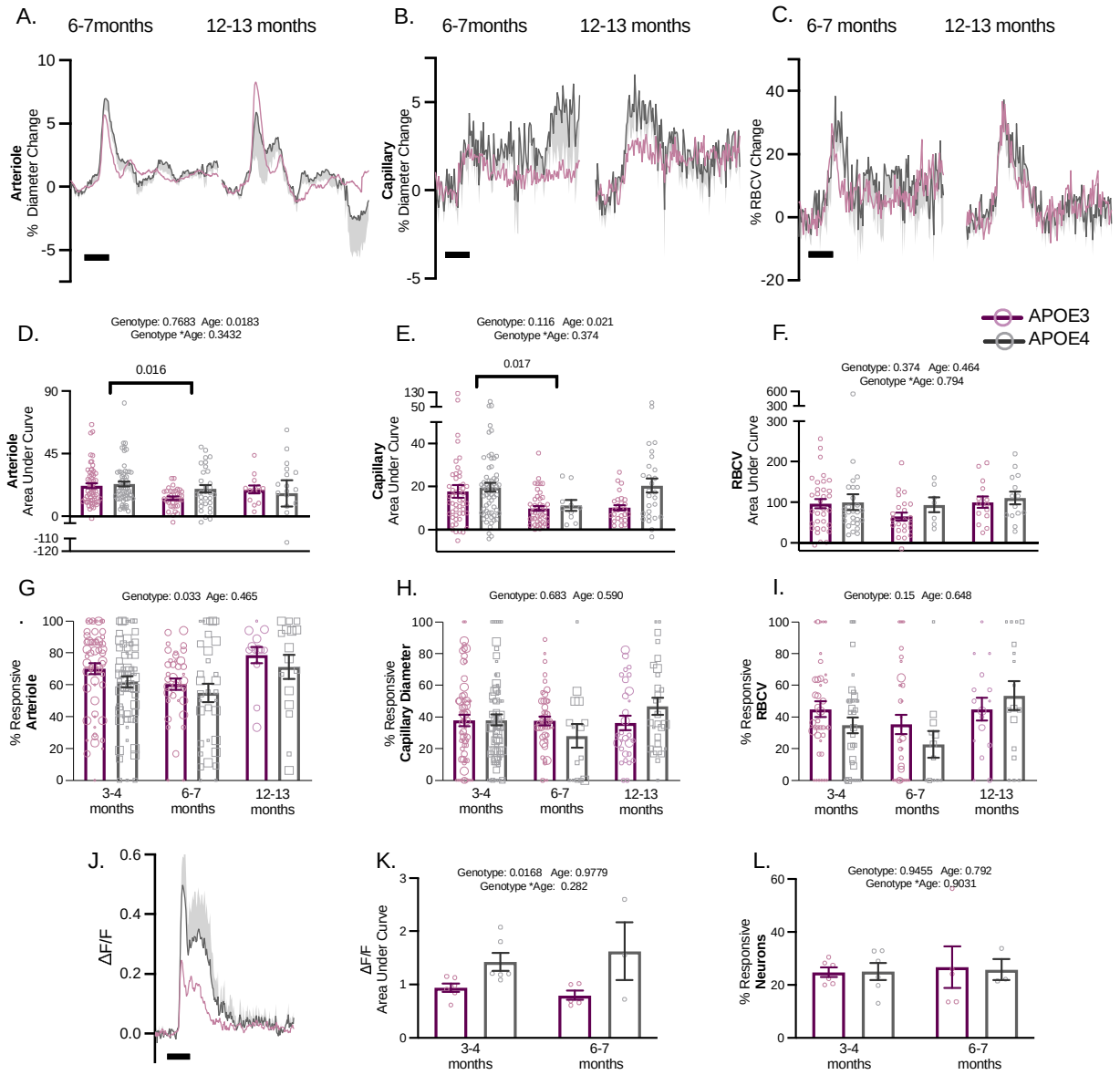

Figure 5. Age does not robustly modulate vascular or neuronal responses to visual stimulation. There was no genotype effect on the response magnitude to visual stimulation in animals across all age points **(A-F)**. In both arteriole diameter and capillary diameter measurements, there was an effect of age, with 3-4 month animals displaying larger responses to stimulation than at 6-7 months, however this effect was not observed in 12-13 month old animals. Response frequency to visual stimulation continued to be modulated by genotype across all ages in arteriole responses to stimulation **(G)**, however they were not affected by age. Neither capillary diameter response frequency **(H)** or RBCV response frequency **(I)** was modulated by age or genotype. At 6-7 months, neuronal responses to stimulation continued to be larger in APOE4 animals **(J, K)**, but this effect was not modulated by age. The response frequency of neurons to stimulation was not affected by age or genotype **(L)**. Data are shown as

mean ± SEM. P values were obtained from LMM with animal ID as a random factor. (D, E, F, K, L) and WLS regression (weighted by number of contributing trials) (G, H, I). Scale bars = 5 s.

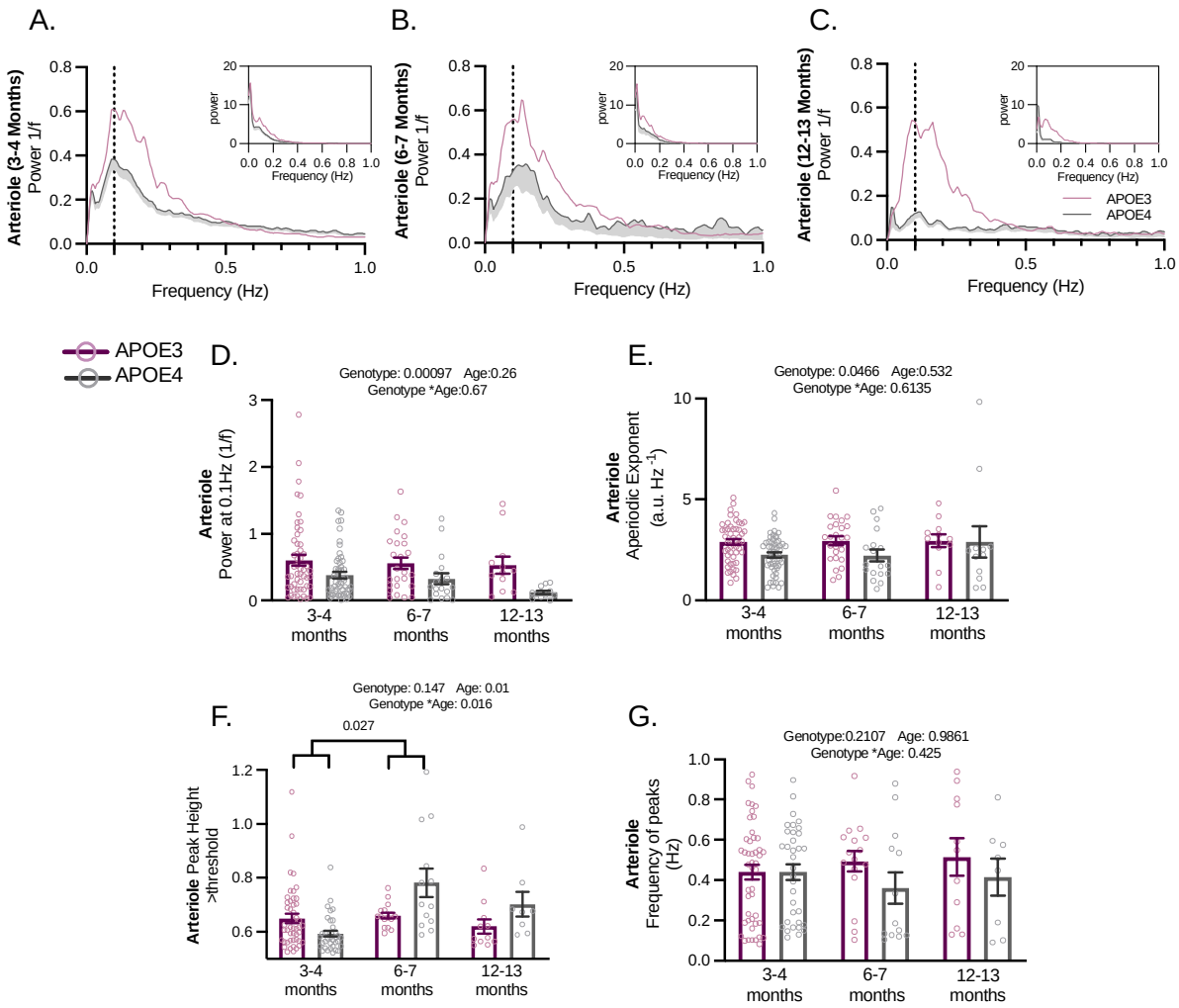

Figure 6. Vasomotion is reduced across all age points but does not appear to be modulated by age. Average power spectra of arteriole diameter traces across all three age points **(A, B, C)**, normalised for 1/f noise (main figure) and unnormalized (insert). APOE4 animals had lower power at 0.1Hz **(D)** and lower aperiodic exponents **(E)**, but these effects did not change with age. Peak height showed an interaction between age and genotype **(F)** (though this may be due to fitting of noise, due to the very low overall power in the older age groups) but the frequency of detected peaks was unchanged **(G)**. Data are shown as mean ± SEM. P values were obtained from LMM with animal ID (D, E) and vessel ID as random factors (F, G). Pairwise comparisons were made with Tukey's correction (F). APOE3/APOE4: (D, E) 3-4 months: n = 52/53 vessels , 15/15 animals, 6-7 months: 25/18 vessels, 10/8 animals, 12-13 months: 12/152 vessels, 4/3 animals. (F, G) 3-4 months: 47/34 peaks, 12/14 animals, 6-7 months: 16/13 peaks, 6/4 animals, 12-13 months: 11/8 peaks, 3/3 animals.

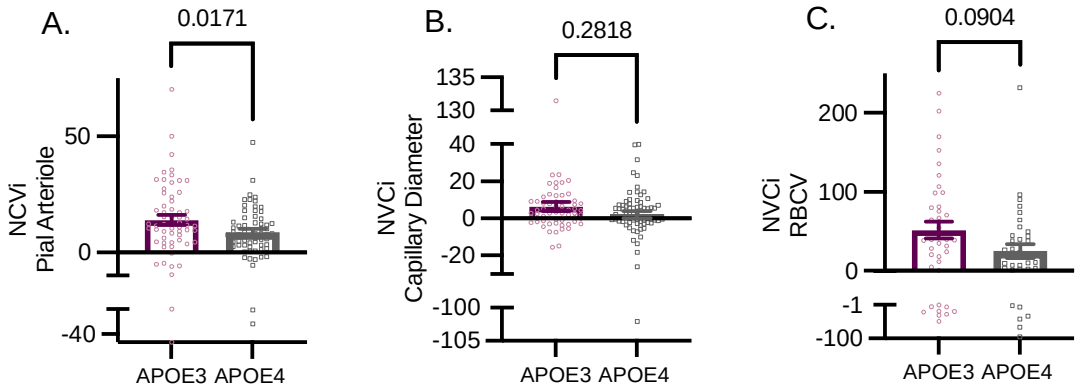

Supplementary Figure 1. Vascular response to visual stimulation normalised to neuronal responses to produce a neurovascular coupling index (NVCi). Raised NVCi in APOE3 animals was observed in pial arteriole **(A)** responses to visual stimulation and at a trend level in RBCV measurements **(C).** No difference was seen in capillary diameter NCVi **(B).**

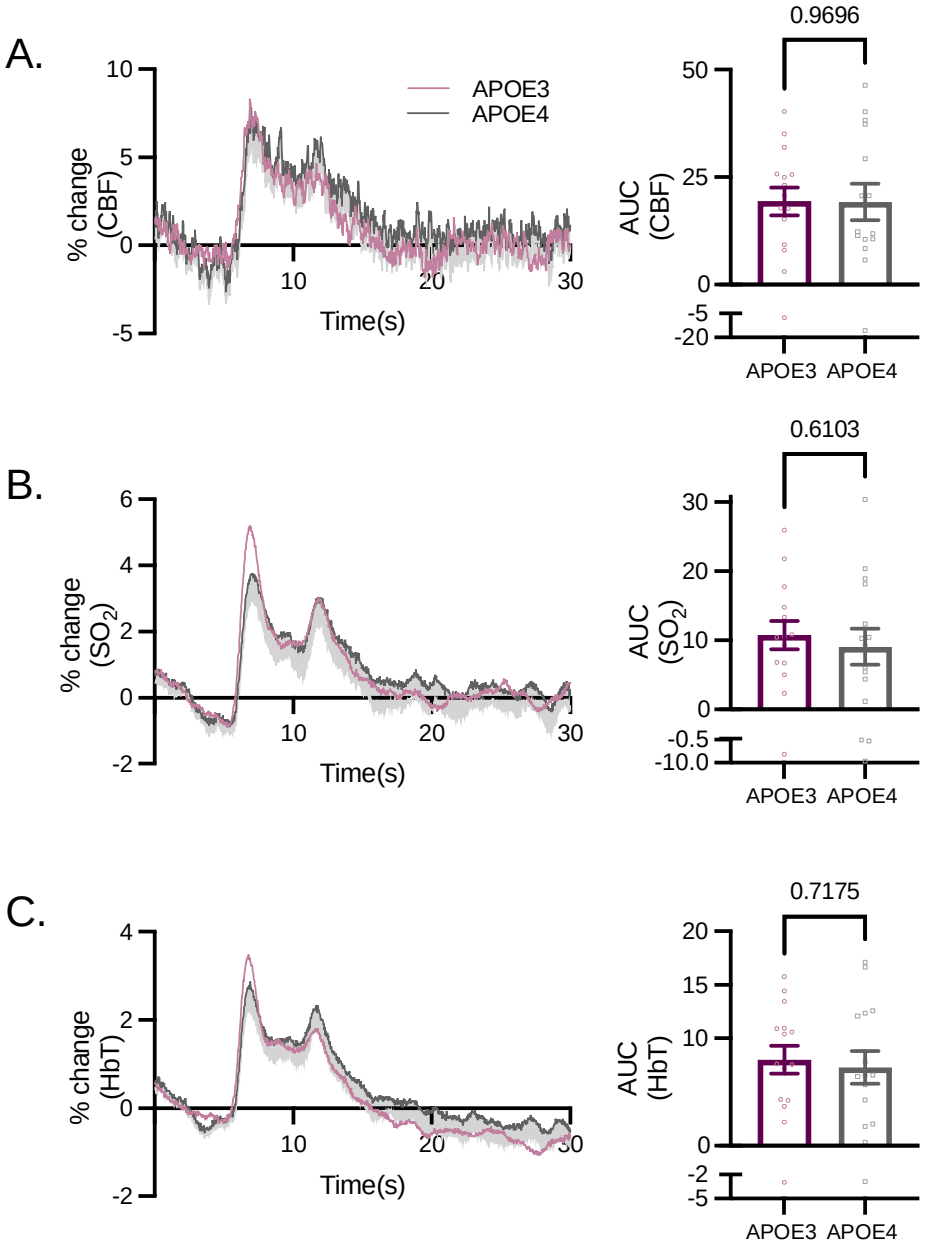

Supplementary Figure 2. No effect of genotype was observed in net measurements: Left panel shows average changes in net CBF **(A)**, sO_2 **(B)** and total haemoglobin (HbT; **C)** during visual stimulation (blue shaded region). Right panel shows AUC for each during visual stimulation. Data are shown as mean ± SEM. P values were obtained from t-tests. APOE3/APOE4: n = 15/15 animals.

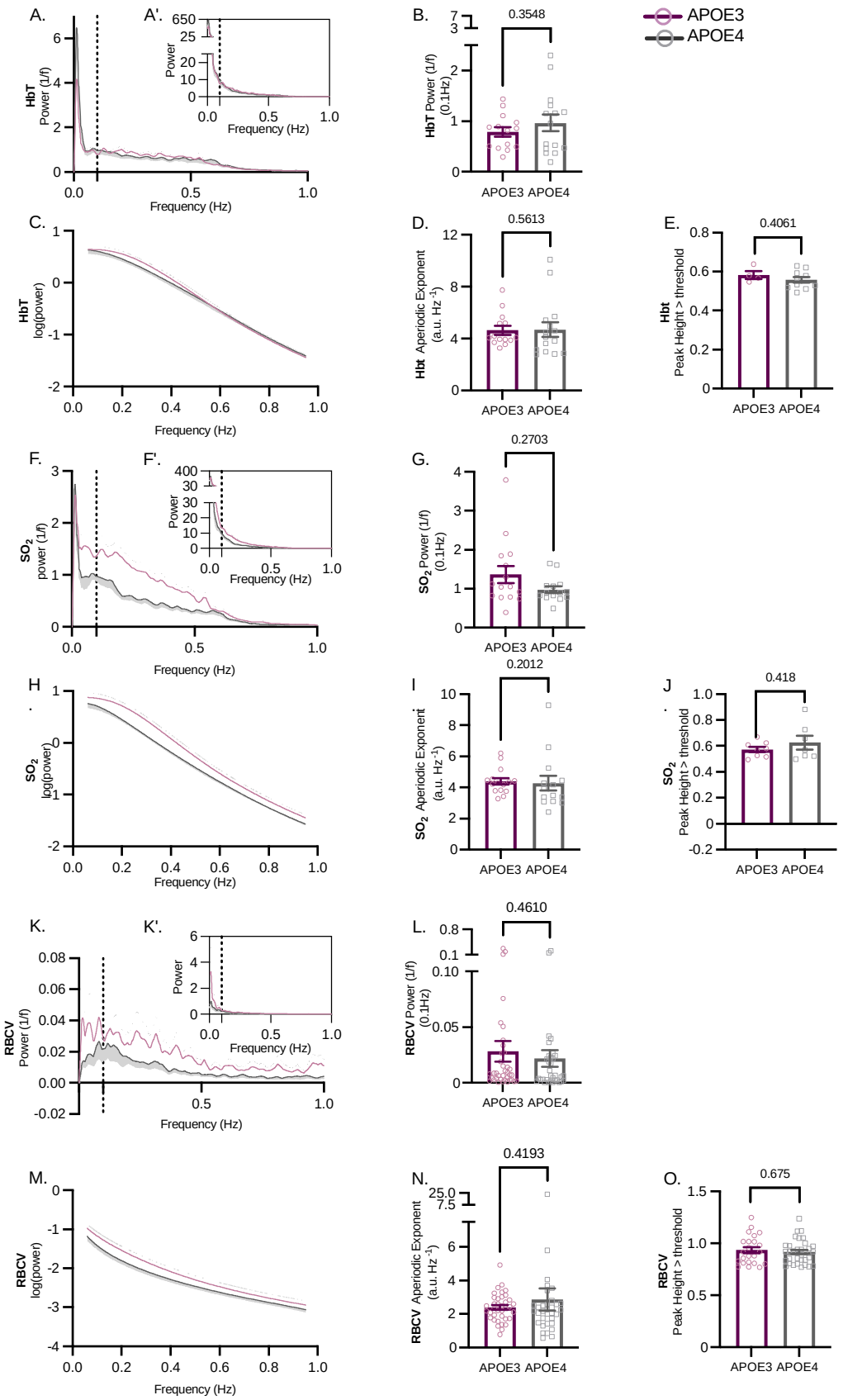
A.
A'.
HbT Power (1/f)
Power
Frequency (Hz)
B.
0.3548
HbT Power (1/f) (0.1Hz)
APOE3 APOE4
APOE3
APOE4
C.
HbT log(power)
Frequency (Hz)
D.
0.5613
Hbt Aperiodic Exponent (a.u. Hz^{-1})
APOE3 APOE4
E.
0.4061
Hbt Peak Height > threshold
APOE3 APOE4
F.
F'.
SO_2 power (1/f)
Power
Frequency (Hz)
G.
0.2703
SO_2 Power (1/f) (0.1Hz)
APOE3 APOE4
H.
SO_2 log(power)
Frequency (Hz)
I.
0.2012
SO_2 Aperiodic Exponent (a.u. Hz^{-1})
APOE3 APOE4
J.
0.418
SO_2 Peak Height > threshold
APOE3 APOE4
K.
K'.
RBCV Power (1/f)
Power
Frequency (Hz)
L.
0.4610
RBCV Power (1/f) (0.1Hz)
APOE3 APOE4
M.
RBCV log(power)
Frequency (Hz)
N.
0.4193
RBCV Aperiodic Exponent (a.u. Hz^{-1})
APOE3 APOE4
O.
0.675
RBCV Peak Height > threshold
APOE3 APOE4

Supplementary Figure 3. No effect of genotype on power was observed in net haemodynamic measurements or in RBCV: No differences in power was observed in total haemoglobin measurements (A, A', B), net sO_2 measurements (F, F', G) and RBCV (K, K', L) at 0.1Hz. No differences in the aperiodic curves or exponents were observed across these parameters (C, D, H, I, M, N) and similarly, there was no difference observed in the size of the peaks above threshold (E, J, O). Data are shown as mean ± SEM. P values were obtained from t-tests ± Welch's correction, Mann Whitney U tests and LMM with vessel ID as a random factor. APOE3/APOE4: (A, B, C, D, F, G, H, I) n = 15/14 animals, (E) n = 5/10 peaks, (J) n = 8/7 peaks, (O) n = 23/33 peaks.

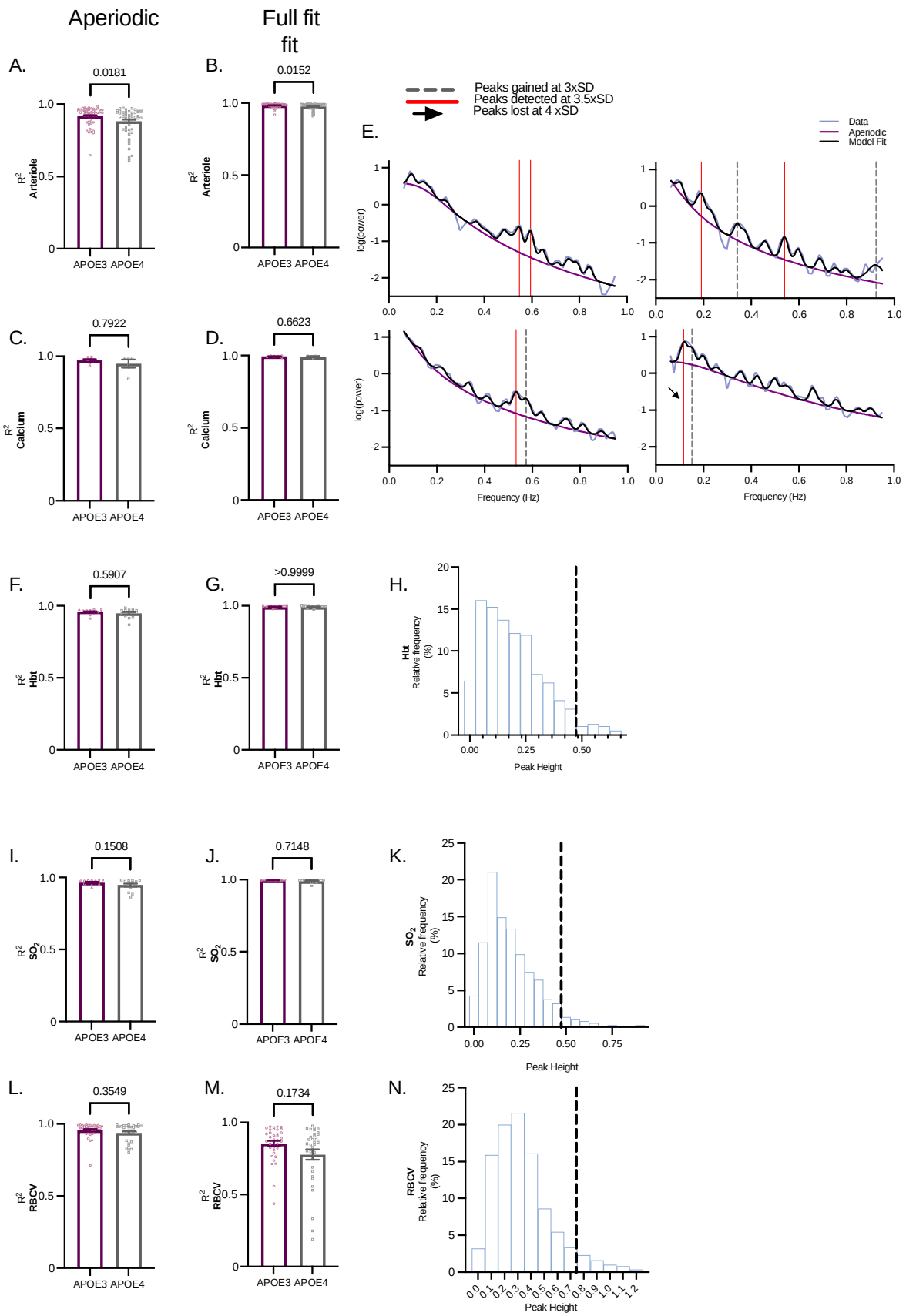
Aperiodic
Full fit
fit
A.
0.0181
B.
0.0152
C.
0.7922
D.
0.6623
E.
Peaks gained at 3xSD
Peaks detected at 3.5xSD
Peaks lost at 4 xSD
Data
Aperiodic
Model Fit
log(power)
Frequency (Hz)
F.
0.5907
G.
>0.9999
H.
Relative frequency (%)
Peak Height
I.
0.1508
J.
0.7148
K.
L.
0.3549
M.
0.1734
N.
APOE3 APOE4

Supplementary Figure 4. Comparison of FOOOF parameters: In pial arterioles, aperiodic **(A)** and full fits **(B)** were lower in APOE4 power spectra compared to APOE3 spectra. This is examined further in S5. For all other parameters (neuronal calcium, (**C, D),** HbT **(F, G),** sO_2 **(I, J),** and RBCV **(L, M)**, there was no difference in goodness of fit. Different thresholds for peak detection are shown in **E)** where red shows the peaks that were detected in the study (3.5 x standard deviation of all peaks), dashed grey lines shows peaks that were detected at a less conservative threshold (3 x standard deviation of all peaks) and the black arrow shows the peak that would be lost with a more conservative threshold (4x standard deviation of all peaks). Histograms for all peaks along with the applied threshold (of 3.5 x standard deviation (dashed line)) are shown for HbT **(H),** sO_2 **(K**) and RBCV **(N).** Data are shown as mean ± SEM. P values were obtained from Mann Whitney U tests or t-tests. APOE3/APOE4: (A, B) n = 52/53 vessels, 15/15 animals, (C, D) n = 1770/1677 cells, 6/5 animals, (F, G, H, I, J, K) n = 15/14 animals, (L, M, N) n = 37/33 vessels, 12/11 animals.

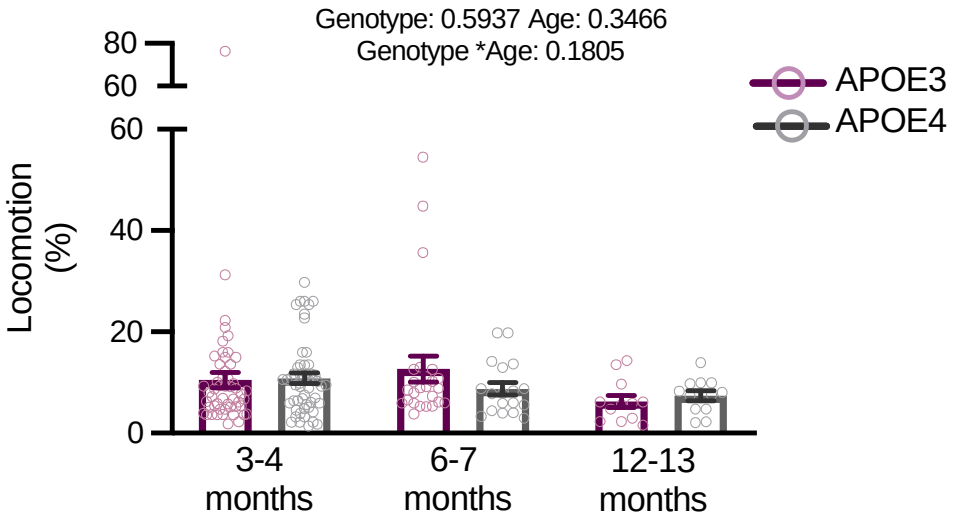

Supplementary Figure 5. No difference in the percentage of time spent engaging in locomotion was observed between time points or genotypes. Data are shown as mean ± SEM. P values were obtained from LMM with animal ID as a random factor. APOE3/APOE4: 3-4 months: n = 52/53 vessels , 15/15 animals, 6-7 months: 25/18 vessels, 10/8 animals, 12-13 months: 12/12 vessels, 4/3 animals.

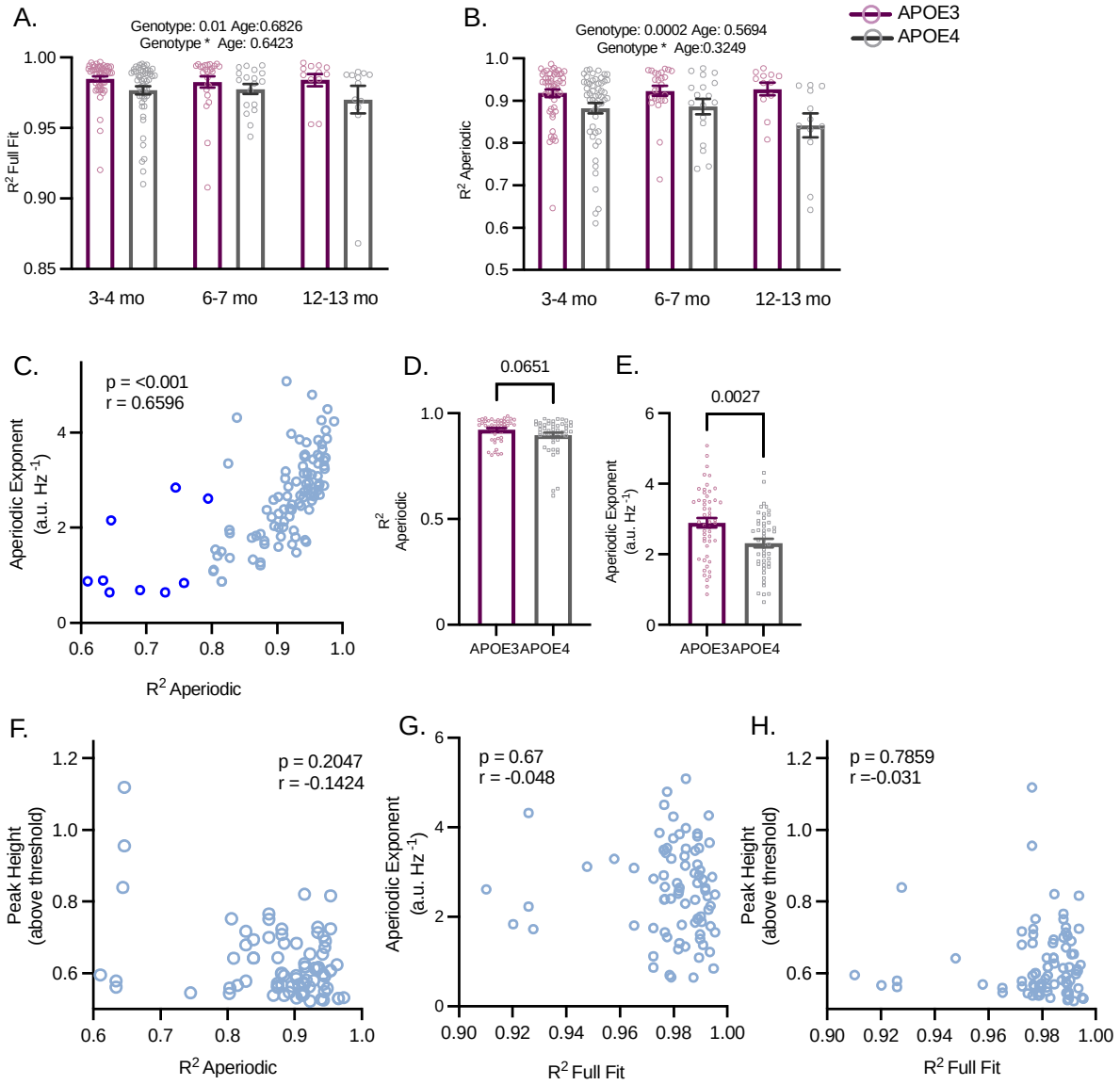

Supplementary Figure 6. In arterioles, the full model fit **(A)** and aperiodic **(B)** goodness of fit are reduced in APOE4 mice across all time points. Data from 3-4 month animals were further analysed to examine the impact of this, and the aperiodic exponent was plotted against the goodness of fit **(C).** There was a significant positive correlation but when all values with a goodness of fit less than 0.8 were removed (dark blue), this removed any genotype difference in the aperiodic goodness of fit **(D),** however the genotype difference in the aperiodic exponent remained **(E).** There was no correlation between the aperiodic goodness of fit and peak height **(F),** the goodness of fit for the full model and the aperiodic exponent **(G)** or the peak height above threshold **(H)**. Data are shown as mean ± SEM. P values were obtained from two- way ANOVA **(A, B),** Pearson's correlation **(C, F**), Spearman's rank correlation **(G, H**), t-test **(D)** and Mann Whitney U test **(E).** APOE3/APOE4 3-4 months: n = 52/53 vessels, 15/15 animals, 6-7 months: 25/18 vessels, 10/8 animals, 12-13 months: 12/12 vessels, 4/3 animals.

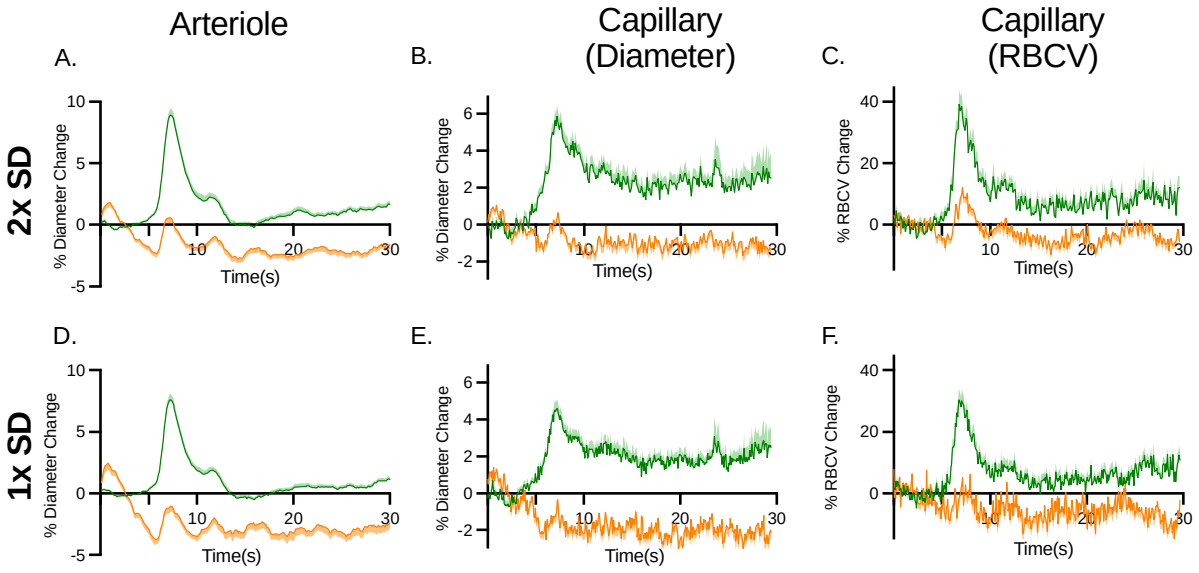

Supplementary Figure 7. Comparison of thresholds for responsive vessels: Mean 'responsive' traces (green) and 'non-responsive' traces (orange) with a threshold of 2x (top panel) and 1x the standard deviation (bottom panel) of the pre-stimulus period in pial arterioles **(A, D),** capillary diameters **(B, E)** and capillary RBCV **(C, F).**

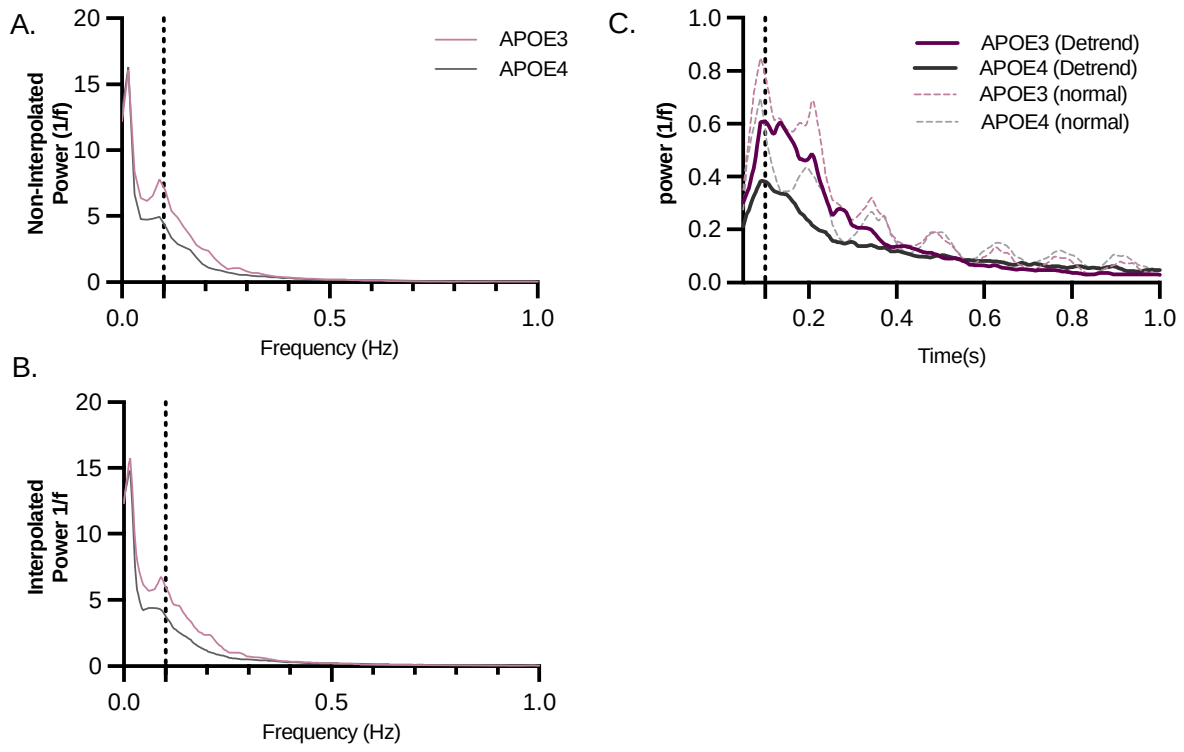

Supplementary Figure 8. Post-processing of data did not alter overall findings. All power spectra data from 3-4 month animals were interpolated and cut at 1Hz to make all traces the same length. **(A)** shows the mean of all APOE3 and APOE4 FFTs before interpolation and **(B)** shows data after interpolation. All data was detrended before Fourier transforms were carried out. **(C)** shows the mean FFT of data without detrending (dashed line) and with detrending (solid lines). APOE3/APOE4 3-4 months: n = 52/53 vessels, 15/15 animals.

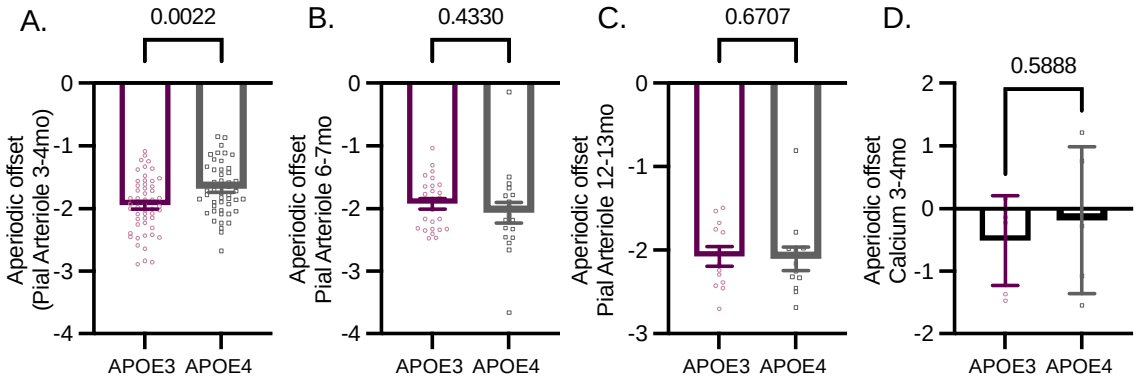

Supplementary Figure 9. Comparison of aperiodic offsets as determined by FOOOF. **A)** APOE3 TR vessels had a lower aperiodic offset in 3-4 month animals. In 6-7 month **(B)** and 12-13 month **(C)** animals, there was no difference between aperiodic offsets. There was also no difference between the aperiodic offsets in calcium measurements. Data are shown as mean ± SEM. P values were obtained from Mann Whitney U tests **(C)** or t-tests **(A, B, D**). APOE3/APOE4: **(A)** n = 52/53 vessels, 15/15 animals, **(B)** n = 25/18 vessels, 10/8 animals**, (C)** n = 12/12 vessels, 4/3 animals(D) n = 1770/1677 cells, 6/5 animals.